

1 **Energetic electron enhancements under radiation belt ($L < 1.2$) during**
2 **nonstorm interval on August 1, 2008**

3 Alla V. Suvorova^{1,3}, Alexei V. Dmitriev^{2,3}, and Vladimir A. Parkhomov⁴

4 ¹ GPS Science and Application Research Center, National Central University, Jhongli, Taiwan

5 ² Institute of Space Science, National Central University, Jhongli, Taiwan

6 ³ Skobeltsyn Institute of Nuclear Physics, Lomonosov Moscow State University, Moscow,
7 Russia

8 ⁴ Baikal State University, Irkutsk, Russia

9
10 *Correspondence to:* Alla Suvorova (suvorova_alla@yahoo.com)

11 **Abstract**

12 An unusual event of deep injections of >30 keV electrons from the radiation belt to low L shells
13 ($L < 1.2$) in midnight-dawn sector occurred during nonstorm conditions on August 1, 2008. Using
14 THEMIS observations in front of the bow shock, we found transient foreshock conditions and
15 rotational discontinuities passing the subsolar region at that time. These conditions resulted in
16 generation of fast magnetosheath plasma jets and penetration of the magnetosheath plasma into
17 the magnetosphere as were observed by the THEMIS probes after approaching the magnetopause.
18 The magnetosphere responded to variations in the IMF orientation by magnetic field
19 perturbations. Magnetic records at ground-magnetometers of INTERMAGNET provided
20 evidence of a global geomagnetic response in the form of geomagnetic pulses from the equator
21 to middle latitudes. The earliest response was found at low latitudes in the predawn sector. We
22 propose a scenario of possible association between dynamical foreshock in the subsolar region,
23 magnetosheath plasma jets and the deepest injections of the >30 keV electrons at $L < 1.2$ at the
24 midnight-dawn sector.

25
26 **Key words:** trapped energetic electrons, low L -shell, magnetosheath plasma jet, foreshock
27

28 **1. Introduction**

29 Deep injections of tens to hundreds of keV particles into the inner magnetosphere, i.e. drift shells
30 $L < 6$, during quiet geomagnetic conditions or weak storm activity have recently become one of
31 the main issues of radiation belt dynamics (e.g., Turner et al., 2017a; Zhao et al., 2017a). The
32 cause of “quiet” injections has not been understood yet. An injection depth is estimated using a
33 notion of drift L-shell, defined by McIlWain (1961). The L parameter determines the unique drift
34 shell, which remains constant when a charged particle moves adiabatically in the inner
35 magnetosphere. Numerically, L gives the average geocentric distance to a drift shell at the
36 magnetic equator. Injection or transport of particles implies violation of adiabatic motion and
37 changing of L-shell.

38 The mechanisms responsible for the violation of adiabatic motion of energetic particles are a
39 subject of extensive modern studies of the radiation belts (e.g., Turner et al., 2015; Turner et al.,
40 2017b; Zhao and Li, 2013; Zhao et al., 2016; Zhao et al., 2017a). The studies presented some
41 intriguing challenges for current models of energetic particle injections in L-shell range of 2-6.
42 Particularly it was pertaining to discrepancy in occurrence frequency, energy range, local time
43 and penetration depth of electron versus proton injections. Zhao et al. (2016) showed that the
44 electrons penetrate into the low L-shells more frequently than protons. In addition, it was found
45 that tens to hundreds of keV electrons penetrate deeper than MeV energy electrons (e.g., Zhao
46 and Li, 2013; Zhao et al., 2016). It was also found that energetic electrons can often penetrate
47 down to the slot region separating the inner and outer radiation belts ($L \sim 2.5 - 3.5$) and also into
48 the inner radiation belt at $L < 2$. Moreover, the deepest penetrations of energetic electrons were
49 revealed even under the inner radiation belt at $L < 1.2$ (Asikainen and Mursula, 2005; Evans,
50 1988; Suvorova et al. 2012; 2013).

51 In the recent study, Zhao et al. (2017a) have compared local time characteristics of electron and
52 proton flux enhancements in the slot region and suggested that underlying physical mechanisms
53 responsible for deep penetrations of protons and electrons are different. Particularly, deep proton

54 penetration is consistent with convection of plasma sheet protons, and deep electron penetration
55 suggests the existence of a local time localized mechanism. Turner et al. (2015) studied energetic
56 electron flux enhancements at $L < 6$ and also suggested that the deep injections at $L < 4$ (inside
57 the plasmasphere) may result from a different mechanism than injections observed at higher L
58 shells (outside the plasmasphere). They hypothesized that the mechanism could be related to
59 wave activity in the Pi2 frequency range which usually serves as an indicator of substorm
60 activity. Overall, dynamics of the tens to hundred keV electrons at low L -shells is very different
61 from dynamics of both protons and electrons at higher L -shells and also in higher energy range.

62 The ability of energetic electrons to penetrate deeply in the inner zone and below is still puzzling.
63 An answer to the question may be found by investigating the relation of deep injections of
64 energetic electrons to solar wind parameters, geomagnetic activity indices and other parameters
65 of magnetospheric and ionospheric responses (Suvorova, 2017; Zhao et al., 2017b). The studies
66 mentioned above have reported deep injections of energetic electrons associated with
67 geomagnetic storms and/or intense substorms, although no significant dependence of penetration
68 depth or flux intensity on the storm intensity was found (e.g., Suvorova et al., 2013; 2014;
69 Turner et al., 2017b; Zhao et al., 2016). Some studies noted that deep injections can occur during
70 nonstorm time but under intense substorm activity (Park et al., 2010; Suvorova et al., 2016;
71 Turner et al., 2015).

72 Extensive studies of dynamics of the energetic electrons in the inner radiation belt and below
73 using the measurements from several satellite missions NOAA/POES, DMSP, DEMETER, and
74 Van Allen Probes (e.g., Reeves et al., 2016; Suvorova, 2017; Turner et al., 2015, Turner et al.,
75 2017a; Zhao and Li, 2013; Zhao et al., 2017a) have revealed the following interesting features
76 such as a high growth rate of fluxes or sudden enhancements, the occurrence of flux
77 enhancements regardless of storm intensity, the influence of solar wind and geomagnetic
78 conditions on the occurrence rate, high occurrences of the injections below the inner zone during
79 specific phases of solar cycles, specific months and local times.

80 Rapid enhancements of electron fluxes in the inner zone have been known for a long time in
81 association with deep injections of particles during strong magnetic storms (e.g., Pfizter and
82 Winckler, 1968; Imhof et al. 1973; Kikuchi and Evans, 1989; Tanaka et al., 1990). As mentioned,
83 recent studies showed that rapid or sudden enhancements deep in the inner magnetosphere
84 cannot be explained by an enhanced convection electric field, convection of plasma sheet
85 electrons or inward radial diffusion (e.g., Turner et al., 2017b; Zhao et al., 2017a). Increased
86 statistics have revealed a feature that deep injections may occur frequently, and furthermore,
87 regardless of storm strength (Tadokoro et al., 2007; Park et al., 2010; Turner et al., 2017a; Zhao
88 and Li, 2013; Zhao et al., 2016). Another important feature, also mentioned above, is that
89 injections of the keV electrons and associated flux enhancements can occur even below the inner
90 belt edge ($L \sim 1.2$), in so-called forbidden zone (Asikainen and Mursula, 2005; Evans, 1988;
91 Suvorova et al., 2012).

92 Until recent years, it was believed that these “forbidden injection” events could occur only
93 during strong magnetic storms and hence could be rarely observed. Note that enhancements in
94 the forbidden zone were first reported in 1960s (Krasovskii et al., 1961; Savenko et al., 1962;
95 Heikilla, 1971), however, the conclusions were unconvincing due to the scarce information (see
96 Paulikas, 1975 for a review). The recent statistical study of electron enhancements in the
97 forbidden zone showed that the injections below the inner zone can also occur during
98 geomagnetically quiet conditions (Suvorova, 2017). This fact is consistent with the recent
99 finding of “quiet” injections in the inner magnetosphere (Turner et al., 2017a; Zhao et al., 2017a).
100 A case of “quiet” injections of energetic electrons at $L < 1.2$ is in the focus of our study.

101 Here, we summarize the main characteristics of the electron injections into the very low L-shells
102 from several papers (Suvorova and Dmitriev, 2015; Suvorova et al., 2013; 2014; 2016; Suvorova,
103 2017; Dmitriev et al., 2017). The quasi-trapped energetic electron population in the forbidden
104 zone, referred to as forbidden energetic electrons (FEE), can be characterized as transient with
105 highly variable fluxes. The behavior of FEE is similar to keV energy trapped electrons in the

106 inner radiation belt with flux enhancements in response to magnetic storms (e.g., Kikuchi and
107 Evans, 1989; Tanaka et al, 1990; Tadokoro et al., 2007; Dmitriev and Yeh, 2008; Zhao and Li,
108 2013; Selesnick et al., 2016). Simultaneous measurements of particles by satellites at different
109 altitudes provided clear evidence that the forbidden zone enhancements of energetic electrons
110 were caused by fast penetration of the inner belt electrons (Suvorova et al., 2014). As known, an
111 important role in fast transport of particles during storms is played by magnetic and electric field
112 perturbations. Such perturbations are usually associated with the influence of magnetospheric
113 substorms, or nighttime processes of magnetic field dipolarizations in the magnetotail (e.g.,
114 Glocer et al., 2011; Selesnick et al., 2016). However, substorm signatures in the magnetic field in
115 the low- L region ($L < 2$) have never been observed.

116 Thus, the deep injections of keV energy electrons may extend even to the forbidden zone, but
117 conditions for the fast ($\sim 1 - 2$ h) earthward transport in the low- L region are still unclear.
118 Nevertheless, the most probable mechanism of the low- L injections of energetic electrons was
119 suggested as the ExB drift (e.g., Suvorova et al., 2012), and most of researchers consider and
120 model an electric drift of electrons in the ExB fields, even though the electric field must be very
121 high (e.g., Zhao and Li, 2013; Turner et al., 2015; Lejosne and Mozer, 2016; Selesnick et al.,
122 2016; Su et al., 2016; Zhao et al., 2017a). [According to simulation results of Selesnick et al.](#)
123 [\(2016\), the electric field of \$\sim 5\$ mV/m can provide deep injections at \$L < 1.3\$.](#) There is no
124 explanation for penetration of a strong electric field to such low L -shells. What is more important,
125 there is no reliable information on electric fields at heights of 500-2000 km, because
126 measurements there are difficult, and, as a consequence of this, empirical electric field models
127 are limited and do not provide the results below $L \sim 2$ (e.g., Rowland and Wygant, 1998; Matsui
128 et al., 2013). The most modern research suggests that the actual strength of penetration electric
129 fields can be stronger than any existing electric field model at $L < 2$ (Su et al., 2016).

130 The studies, mentioned above, have also analyzed a relation between the FEE injections and
131 geomagnetic activity level. It seemed for a while that intense geomagnetic activity like auroral

132 substorms was one of the necessary factors for deep electron injections, and the storm-time *Dst*-
133 variation did not control the FEE occurrences (Suvorova et al., 2014). It was suggested that
134 substorm-associated strong electric field can penetrate to the low *L* region, thereby creating the
135 conditions for fast earthward transport of trapped electrons in crossed E and B fields. Recent
136 modeling of the ExB transport mechanism at $L < 1.3$ demonstrated that the mechanism can
137 successfully operate in the low *L* region (Selesnick et al., 2016).

138 However, after that, many FEE events were found during moderate and weak auroral activity,
139 which was typical for pre-storm (initial phase) or even non-storm conditions (Suvorova and
140 Dmitriev, 2015; Suvorova et al., 2016). Thus, though no evidence of direct influence of
141 geomagnetic storms was found, the FEE enhancements appeared to be necessarily associated
142 with substorm activity in some events studied (Suvorova et al., 2014; 2016). However,
143 statistically, such a casual relationship with substorms was not confirmed (Suvorova, 2017).
144 From total statistics of ~530 days with FEE enhancements collected during two solar cycles
145 (Suvorova, 2017), we found more than three dozen days without essential substorm activity.
146 These “quiet” events occurred over past decade from 2006 to 2016. The FEE enhancements in
147 that case were observed only in low energy range of tens of keV.

148 It is important to mention that one interesting feature was unexpectedly found from the statistical
149 study (Suvorova, 2017). It is that the most favorable conditions for the FEE enhancements arise
150 in the period from May to September independently on geomagnetic activity level. A second,
151 minor peak of occurrence appears in the December - January period. Suvorova (2017) suggested
152 an important role of the auroral ionosphere in the occurrence of FEE injections. The peculiar
153 annual variation of the FEE occurrence rate was explained by a change in conductance of the
154 auroral ionosphere. The conductance depends directly on the illumination of the noon sector of
155 the auroral zone. As known, the high-latitude ionosphere is better illuminated during solstice
156 periods, with that the illumination of the northern region is higher than the illumination of the
157 southern one because of the dipole axis offset relative to the Earth’s center. This fact can explain

158 an existence of two peaks of the FEE occurrence with the major one during the northern summer
159 period.

160 External drivers from the solar wind should trigger some processes in the magnetosphere-
161 ionosphere system that might result in the electron injections into the forbidden zone. However,
162 the external drivers are necessary but often not sufficient for FEE enhancements to occur. If the
163 auroral ionosphere is sunlit, then impact of external drivers more likely results in the electron
164 injections into the forbidden zone. In this case, the factor of the dayside auroral ionosphere
165 conductivity is sufficient, and it comes to the fore during weak geomagnetic activity. The
166 relevant processes in the magnetosphere-ionosphere chain during magnetic quiet are still unclear.
167 A comprehensive analysis of the solar wind drivers and magnetospheric response may help us to
168 lift the veil. In this paper, we study prominent FEE enhancements during nonstorm condition on
169 August 1, 2008 in order to determine their possible drivers in the solar wind. Note that this event
170 is a subset (1%) of the total statistics collected by Suvorova (2017) during various conditions,
171 from magnetic quite to extremely strong geomagnetic storms.

172

173 **2. Observations on August 1, 2008**

174 **2.1. Forbidden Electron Enhancements**

175 Figure 1 shows large enhancements of the >30 keV electron fluxes at low latitudes on August 1,
176 2008. The data were compiled from all orbital passes of five NOAA/POES satellites. The
177 electron fluxes in the energy ranges >30 , >100 and >300 keV were measured by the MEPED
178 instruments boarded on each satellite. The MEPED instrument includes two identical electron
179 solid-state detector telescopes and measures particle fluxes in two directions: along and
180 perpendicular to the local vertical direction (Evans and Greer, 2004). The data shown in Figure 1
181 are from the detector was oriented along the orbital radius-vector (i.e. vertically), so that it
182 measured quasi-trapped particles near the equator and precipitating particles in the auroral region.
183 In Figure 1, the forbidden zone extends at $L < 1.2$ in the latitudinal range from -20° to $+30^\circ$ and

184 in the longitudinal range from 0° to 260°E (or 100°W) that is beyond the South Atlantic anomaly
185 (SAA). Figure 1a shows the observations of the >30 keV electrons at 0 - 12 UT, before the
186 enhancements occurred. At that time, the satellites passed the same regions but they did not
187 detect any FEE enhancements. Figure 1b shows the interval 12 - 24 UT, when fluxes of >30 keV
188 quasi-trapped electrons in the forbidden zone increased by 3 orders of magnitude above a
189 background of $\sim 10^2$ ($\text{cm}^2 \text{ s sr}^{-1}$). We have selected FEE enhancements with intensity $>10^3$ ($\text{cm}^2 \text{ s}$
190 sr^{-1}). As found previously, the flux enhancements at low latitudes are peculiar to the quasi-
191 trapped energetic electrons (Suvorova et al., 2012, 2013). In contrast, enhancements of electrons
192 precipitating at low latitudes are very rare, weak and short. During the event, precipitating
193 electron fluxes in the forbidden zone did not increase (not shown). Fluxes of the >100 keV
194 electrons and >30 keV protons did not increase also (not shown). The quasi-trapped electrons are
195 mirroring at heights below the satellite orbit (~ 850 km) in a region of $\pm 30^\circ$ latitudes, and drift
196 eastward with a rate of 17° - 19° per hour toward the SAA area, where they are lost due to
197 scattering in the dense atmosphere.

198 Figure 2 and Table 1 present main characteristics of 15 FEE enhancements detected along
199 equatorial passes of POES satellites (P2, P5, P6, P7, P8). The fluxes kept at the enhanced level
200 for several hours. We analyze the peak fluxes in the FEE enhancements (time, local time,
201 longitude, and L-shell). Positions of the satellite orbital planes provided a good coverage of the
202 entire local time (LT) range: 9 - 21 LT (P2 and P7), 5 - 17 LT (P5 and P6), and 2 - 14 LT (P8).
203 The coverage allows determining the injection region with uncertainty of approximately 2 h. The
204 first FEE enhancement was observed at ~ 1250 UT in Central Pacific at night time (2 LT), and
205 the last (enhancement number F15) was detected at ~ 2310 UT near the western edge of SAA at
206 day time (17 LT). As seen in Figure 2a,b, the FEE enhancements peak at minimal L-shells, i.e. at
207 the equator. The fluxes decrease quickly with growing L. This pattern corresponds to a fast radial
208 transport (injection) of electrons from the inner radiation belt. Note that pitch-angular scattering

209 of electrons gives different profiles: the fluxes should be minimal and the equator and grow with
210 L-shell.

211 It was shown statistically that deep injections into the forbidden zone, similar to plasma sheet
212 particle injections, occur in the midnight - morning sector (e.g., Suvorova, 2017). During typical
213 geomagnetic disturbances, nighttime FEE enhancements are observed shortly after local
214 injections and near an injection site, while subsequent FEE enhancements at daytime are already
215 the result of azimuthal drift of electrons injected on the nightside. Hence, the nighttime (~ 2 LT)
216 enhancements F1 and F4 of >30 keV electron fluxes indicate approximately the time of injection,
217 respectively, at ~ 1250 and ~ 1430 UT or a little bit earlier. After 1530 UT, enhancements were
218 observed at daytime (numbers F7, F9, and F11-15) and are therefore associated with drifting
219 electrons.

220 All remaining enhancements F2, F3, F5, F6, F8 and F10 of >30 keV electron fluxes were
221 observed in the early morning (5 LT) for a long time interval of ~ 4 h that lead us to suspect that
222 the enhancements were observed near the injection site. Nevertheless, we examine the
223 assumption about drift by comparing these enhancements with the injection time for numbers 1
224 and 4 in Table 1. For the enhancements F1 and F2, 30 keV electrons injected at 1250 UT must
225 drift $\sim 35.4^\circ$ of longitude in order to reach the observing satellite P5. It takes ~ 112 min with the
226 drift rate of $19^\circ/\text{h}$ for 30 keV electrons at $L \sim 1.2$ or 125 min with the drift rate of $17^\circ/\text{h}$ at $L \sim 1.1$.
227 However, the observed time difference between F1 and F2 is only 25 min that is too short for
228 drifting from the longitude of F1 to the longitude of F2.

229 The enhancements F1 and F3 have the longitudinal difference of 26° for 1 h that is much larger
230 than 19° produced by the drift of >30 keV electrons. Either it could be electrons of slightly
231 higher energy of ~ 40 - 50 keV. However, intensity of these electrons is several times lower than
232 that for 30 keV electrons because of very steep energy spectrum with maximum in the range of
233 20-30 keV as shown in the previous study (Suvorova et al., 2013). In contrast, the observations

234 did not show notable flux decrease. It means that vast majority of the POES/MEPED count rate
235 is produced by electrons of ~ 30 keV.

236 Likewise, one can infer that the enhancement F4 also did not result in the enhancements F5 and
237 F6 and certainly not in the enhancements F8 and F10. Therefore, the specific longitudinal and
238 local time distributions of the enhancements indicate multiple injections during about 4.5 h in the
239 sector of 0 - 6 LT, and the injection region was confined within 3 h of local time over central and
240 eastern Pacific. In general, these characteristic of injections are in well agreement with those
241 found from statistics (Suvorova, 2017).

242

243 **2.2. Upstream Solar Wind Conditions**

244 An intriguing aspect of these FEE injection events is that they occurred under quiet, nonstorm
245 conditions, characterized by Dst/SYM-H ~ 0 nT and AE < 100 nT. We examine solar wind
246 parameters to search for drivers inducing such deep electron injections. In the study, we focus on
247 a comparison between the solar wind parameters measured far upstream and near the bow shock
248 and on their influence on the magnetospheric magnetic field during the period of interest. Global
249 indices of geomagnetic activity and solar wind data from the Omni high-resolution data set are
250 shown in Figure 3. The OMNI data base provides solar wind data, which were originally
251 obtained from upstream monitors (e.g., ACE or Wind satellites) near the L1 libration point at
252 geocentric distance of ~ 230 Re (Re is the Earth's radius), and then the data were corrected by
253 time delay procedure due to propagation to the Earth's bow shock (King and Papitashvili, 2005).

254 As seen in Figure 3, the solar wind speed and density smoothly varied around averages of 400
255 km/s and 6 to 4 cm⁻³, respectively, that resulted in gradual change of the dynamic pressure Pd
256 from 2 to 1 nPa. The interplanetary magnetic field (IMF) can be characterized as weakly
257 disturbed by small-scale structures because of chaotic variations of the magnetic field
258 components and discontinuities, particularly during the first half of the day. Also, in this period,

259 the Bz component was predominately positive. Later, there was a short interval from 1500 to
260 1800 UT, when IMF orientation was relatively steady with a continuous negative Bz of about -2
261 nT. Likely, the southward IMF resulted in intensification of the AL index from 16 to 18 UT with
262 a peak of -250 nT. The 1 min SYM-H index was > -10 nT throughout the whole day, indicating
263 there was no geomagnetic storm. Therefore, the solar wind conditions resulted in a weak auroral
264 disturbance like an isolated substorm.

265 Overall, the OMNI magnetic and plasma parameters can be characterized as almost undisturbed
266 in the period of the FEE enhancements from 1200 to 2300 UT. Obviously, the weak auroral
267 activity at ~1700 UT could not result in extremely deep injections of the energetic electrons,
268 which started much earlier, around 1300 UT. Whereas, looking on the PC index, which
269 represents magnetic activity in the northern (PCN) and southern (PCS) polar caps (Troshichev et
270 al., 1988), one can see a clear disturbance, particularly in the northern polar cap, in the period
271 from 1300 to 1530 UT. But it's difficult to identify appropriate solar wind drivers for
272 interpretation of this polar cap activity.

273 This raises the question of actual solar wind characteristics at the near-Earth location during the
274 event. The FEE enhancement event under the nonstorm condition and mild, ordinary solar wind
275 properties presents intriguing challenge to current understanding of the deep energetic particle
276 injections, which usually are associated with intense substorm activity. From the characteristic
277 PC-index behavior, we suspect the actual solar wind parameters affecting the magnetosphere
278 may be different from those predicted by OMNI. Fortunately, the near-Earth THEMIS mission
279 can provide necessary reliable information on upstream conditions.

280

281 **2.3. THEMIS foreshock observations**

282 During the time interval from 1200 to 1800 UT, the THEMIS-C satellite (TH-C) had a position
283 upstream of the bow shock in the subsolar region (Figure 4). The TH-C probe moved from

284 location (17.2, -0.3, -5.9) Re in GSM at 1200 UT to location (18.1, 3.4, -5.9) Re at 1800 UT.
285 Hence, we can evaluate characteristics of the upstream solar wind structures actually affecting
286 the magnetosphere during the period of the FEE enhancements. Figure 5a shows measurements
287 of the THEMIS-C/FGM fluxgate magnetometer in GSM coordinates with a time resolution of ~3
288 s (Auster et al., 2008) and the ion spectrograms from THEMIS-C/ESA plasma instrument
289 (McFadden et al., 2008). The magnetic field components measured in situ by TH-C are
290 compared with those predicted by OMNI and shown in Figure 5b. Also, Figure 5c presents the
291 IMF cone angles, between the IMF vector and the Earth-Sun line, for both magnetic data sets.

292 From 1200 UT to 1320 UT, three TH-C magnetic components demonstrated small-amplitude
293 variations, and the Bz component had northward direction. During this time, there were
294 discrepancies between magnetic components of the TH-C and OMNI data caused mostly by time
295 shift of ~10-15 min, so that TH-C observed arrival of the solar wind structures at earlier time
296 than that predicted by OMNI. With time correction, one can achieve better consistency in the
297 two magnetic data sets except the difference in the Bx components about 1310 UT.

298 In Figure 5c, the OMNI cone angle dropped below 30° between 1330 and 1520 UT that
299 corresponded to quasi-radial IMF orientation (IMF is almost along the Earth-Sun line), whereas
300 cone angle variations detected by TH-C were very different from the OMNI data. After 1500 UT,
301 the OMNI data do not match the TH-C observation any more, even with time correction. About
302 ~1320 UT, ~1400 UT and after 1440 UT, the in-situ observation of THEMIS shows large-
303 amplitude fluctuations with duration of tens of minutes in three magnetic components and cone
304 angle (Figure 5a, c). The observed large magnetic fluctuations are ultralow-frequency (ULF)
305 waves, and they are a typical signature of the upstream region of quasi-parallel bow shocks, so-
306 called foreshock (e.g., Schwartz and Burgess, 1991). In addition, in the same time intervals, the
307 plasma spectrogram shows enhancements of suprathermal ion fluxes with energy of >10 keV
308 (upper panel in Figure 5a). This is another distinguishing signature of the foreshock, known as
309 diffuse ion population, which is always observed together with the upstream ULF waves

310 (Gosling et al., 1978; Paschmann et al., 1979; Greenstadt et al., 1980; Crooker et al. 1981).
311 Hence, the upstream foreshock waves and diffuse ions observed by TH-C in the subsolar region
312 are associated distinctly with a radial or quasi-radial IMF orientation in the undisturbed solar
313 wind. Note, that the longest foreshock interval (1435 - 1550 UT) associated with the quasi-radial
314 IMF orientation was observed by ~20 min later than that predicted by OMNI.

315 After 1520 UT, the prediction and in-situ data mismatch greatly. The TH-C satellite observed
316 several rotational discontinuities and alternation between Archimedean spiral and radial
317 orientations of the IMF vector, while the OMNI magnetic field does not change the Archimedean
318 spiral orientation from 1520 to 1740 UT. The foreshock returned to the subsolar region
319 periodically and more frequently in the interval 1600 - 1730 UT than in the earlier period 1320 -
320 1440 UT.

321 These two time intervals of frequent foreshock transitions differ in the B_z component: $B_z > 0$ at
322 1320 - 1440 UT and $B_z < 0$ at 1600-1700 UT. It's natural, that the southward B_z results in the
323 weak auroral activity during the later interval. Nevertheless, the changing direction of IMF has
324 the effect on the magnetic activity in the northern polar cap in the both interval (see the PC index
325 in Figure 1). We check available satellite and ground-based magnetic data to find other responses
326 inside the magnetosphere to the foreshock transitions.

327

328 **2.4. Magnetospheric magnetic field perturbations**

329 We use magnetic field and plasma measurements in the magnetosphere from the other three
330 THEMIS probes and GOES-12 satellite in order to find signatures of local magnetospheric
331 disturbances. With these data, we examine a magnetospheric response to the subsolar foreshock,
332 which forms each time with arrival of magnetic flux tubes with quasi-radial IMF orientation.
333 Positions of the TH-B, TH-D, TH-E and GOES-12 satellites in the X-Y GSM plane for the
334 period from 1200 to 1800 UT are shown in Figure 4. We used the model of Lin et al. (2010) to

335 calculate magnetopause position. The OMNI data at 1600 UT is used as input data for the model.
336 The GOES12 satellite moved from morning to noon (7 - 13 LT). The TH-E and TH-D probes
337 moved outward from prenoon to postnoon, and the TH-B probe moved inward in the afternoon-
338 dusk sectors.

339 Figure 6 shows variations of the Bz component measured by the TH-E, TH-D, and TH-B probes,
340 the magnetic field strength at geosynchronous orbit (GOES-12), the ion spectrogram from the TH-
341 D satellite and the SYM-H index from 1200 to 1800 UT. As seen in Figure 6 (a, d),
342 characteristics of magnetic field and hot plasma indicate that three THEMIS probes were located
343 inside the dayside magnetosphere during the interval, a region of a strong magnetic field with the
344 magnitude ranging from 40 to 150 nT and low-density of hot (>10 keV) ions. Three THEMIS
345 probes observed significant perturbations in the magnetic field Bz component with
346 increase/decrease of order of several to tens of nT. After 1400 UT, the largest amplitudes were
347 observed by TH-D, which was closer to the magnetopause than other probes at that time (see
348 Figure 4). From 1300 to 1500 UT, there are a few characteristic decreases and enhancements in
349 the Bz component with duration of 20-30 min observed by all probes (Figure 6a). The magnetic
350 field increases correspond to magnetospheric compressions, and the decreases are
351 magnetospheric expansions (e.g., Dmitriev and Suvorova, 2012). Prominent magnetic peaks are
352 indicated by dashed lines and listed in Table 2. At ~1700 and 1715 UT, the TH-D measurements
353 show that the sign of the Bz component suddenly reversed for a few minutes. The negative Bz
354 component is a clear signature of the magnetosheath magnetic field. We will consider details of
355 the magnetosheath intrusion events later.

356 As seen in Figures 6a-c, THEMIS magnetic observations well correlate with magnetic field
357 variation observed by GOES-12 and with the SYM-H index in the interval 1300-1600 UT. The
358 first magnetic pulse was observed at ~13:33:40 simultaneously by TH-B, TH-E, and TH-D and
359 with a delay of ~2 min by GOES 12. Time moments of magnetic peak 2 coincide for all satellites
360 (14:20:50 UT). Magnetic peak 3 was observed at first by GOES 12 at ~15:44:00 (~10.6 LT),

361 then by TH-E at ~15:47:30 (~12 LT) and at last by TH-D at ~15:50:30 UT (~12.5 LT), so a time
362 difference between GOES 12 and TH-D is ~ 6.5 min and between TH-E and TH-D is 3 min.

363 The magnetic variations associated with compression-expansion effects could not be caused by
364 the solar wind pressure variations, which were gradual and small during the interval (see Figure
365 3). However, the magnetic perturbations may result from local variations in the magnetosheath
366 pressure. Unfortunately, THEMIS did not measure plasma parameters in the magnetosheath from
367 1200 to 1600 UT, but an analysis of the later interval (1600-1800 UT) can provide important
368 information about magnetosheath conditions (see also section 2.5).

369 After 1545 UT, the TH-D probe observed fast magnetic variations. At that time the probe was
370 approaching the magnetopause and moving ahead of the TH-E probe (see Figure 4). Note, that
371 the fast magnetic fluctuations are not always seen in SYM-H and GOES 12 data because of a
372 low time resolution (1 min) of these data. Figure 6d presents the ion spectrogram from TH-D.
373 One can see several short-time intrusions of dense and cold plasma with spectrum typical for the
374 magnetosheath. Moreover, at ~1700 and 1710 UT, the magnetospheric field measured by TH-D
375 with positive B_z suddenly overturned to negative B_z for a moment that indicated a
376 magnetosheath encounter. Time moments of peaks in the magnetosheath plasma pressure are
377 indicated by lines 4-10 in Figure 6 and listed in Table 2. Below, we analyze characteristics of
378 magnetosheath ions in details.

379

380 **2.5. Magnetosheath plasma jets interacting with the magnetopause**

381 We analyze the solar wind characteristics in the foreshock region together with the
382 magnetospheric magnetic perturbations and penetration of magnetosheath ions. Figure 7 shows
383 the magnetic field and plasma parameters observed by TH-D, TH-E and TH-C during the
384 interval 1530-1800 UT. In addition, magnetic measurements from GOES 12 and geomagnetic
385 indices are also shown.

386 After 1530 UT, the TH-D and TH-E probes have observed magnetic field pulses associated with
387 the compression effect (Figure 7g). After 1600 UT, TH-D was approaching the magnetopause
388 and started observing occasionally magnetosheath plasma in the magnetosphere, as seen in the
389 ion spectrogram (e.g., lines #4 – 7 and 10, Figures 7b). After 1700 UT, the probe twice entered
390 into and exited from the magnetosheath region as indicated by lines #8 and #9. The
391 magnetosheath plasma can be recognized as dense and cold (<1 keV) ion population. As seen in
392 Figure 7 (panels b and g), not all magnetic pulses are accompanied by plasma penetrations.
393 During the interval, the outermost probe TH-C observed occasionally the foreshock phenomena
394 such as diffuse ions (≥ 10 keV) in the spectrum (panel a) and large IMF cone angle fluctuations
395 associated with ULF waves (panel h). As one can see, most of the magnetic pulses (panel g)
396 and/or magnetosheath ion populations (panel b) indicated by lines #3, #4, and #6-10 (i.e. except
397 #5) were accompanied by the foreshock diffuse ions (panel a).

398 Figure 8 shows characteristics of magnetosheath plasma in details for three intervals 1600-1630,
399 1630-1700, and 1658-1728 UT. Since plasma charge neutrality means equal density of ions and
400 electrons, Figure 8 presents parameters of the ion component only (panels a-d). Total pressure
401 (P_{tot}) and density (D) of the solar wind plasma measured far upstream by the ACE monitor are
402 also shown for comparison in panels (b, c). The time period from 1600 to 1630 UT is shown in
403 panels (a1-g1). The probes TH-D and TH-E observed magnetic field variation in specific
404 depletion-hump sequence from 1607 to 1614 UT (panels f1, g1), similar to the variations
405 indicated by lines #1 - #3 in the earlier interval (see Figure 6). Magnetic peak is indicated by line
406 #4. Additionally, wave-like structures with a period of ~ 30 -60 sec (in the ULF range) are clearly
407 seen in magnetic measurement of both probes during the time interval from 1609 to 1627 UT
408 (panels f1, g1). At 1614 - 1616 UT, TH-D observed cold ions (~ 100 eV - 3 keV) and electrons
409 (<1 keV, not shown) of the magnetosheath origin staying in the magnetosphere (panel a1). The
410 plasma has maximal speed of >200 km/s and high density of 3 -9 cm^{-3} that result in the high total
411 pressure of 1.5 - 1.8 nPa (panels b1-d1). Its dynamical characteristics distinctly exceed the solar

412 wind parameters with density of $4 - 5 \text{ cm}^{-3}$ and total pressure of $\sim 1.1 \text{ nPa}$ (panels b1, c1). Internal
413 structure of plasma forms 3 prominent pressure pulses between 16:14:50 and 16:16:00 UT, a
414 central pulse is dominated by magnetic component (panel f1) and two lateral pulses are
415 dominated by dense plasma components (panel c1). Two plasma density enhancements produced
416 a diamagnetic effect seen as a characteristic decrease of magnetic field (panel f1). At the outer
417 edge of the plasma structure, the anti-sunward velocity ($V_x < 0$) reached high value of -100 km/s ,
418 indicating that the local plasma flow struck and interacted with the magnetopause (panel d1).
419 The V_z component demonstrates a maximal value in southward direction (-200 km/s). Three
420 rotated velocity components V_x , V_y and V_z indicate that vortex-like plasma structure propagated
421 along the magnetopause toward south and dusk. This dense and high-speed plasma structure is
422 analogous to the large-scale magnetosheath plasma jet studied by Dmitriev and Suvorova (2012).
423 Large-scale magnetosheath plasma jets are defined as intense localized fast ion fluxes whose
424 kinetic energy density is several times higher than that in the upstream solar wind and duration is
425 longer than 30 sec (Dmitriev and Suvorova, 2015).

426 Panels (a2-g2) in Figure 8 show magnetic compressions and magnetosheath penetrations (lines
427 #5 - #7) during the time period from 1630 to 1700 UT. It is also seen that the magnetic field
428 measured by TH-E was disturbed by ULF wave activity (panel g2). The plasma structures #5 and
429 #6 (panel a2) have short durations and are characterized by extremely high density of 16 and 12
430 cm^{-3} , respectively, that well explain the compression effects in magnetic measurements from TH-
431 E and TH-D (panels f2, g2). Prolonged plasma structure #7 has lower density of $4 - 9 \text{ cm}^{-3}$ and
432 did not produce a notable compression effect in accordance with to TH-E magnetic
433 measurements (panel g2). It is important that inside each plasma structure, we reveal a dense
434 plasma core, which is characterized by enhanced speed of ~ 150 or $\sim 220 \text{ km/s}$ with a dominant
435 V_z component (negative or positive). These parameters, typical for plasma jets, formed pressure
436 of high magnitude, which exceeded the upstream solar wind pressure by 50-80 % (panel b2).
437 Likely, magnetosheath plasma jets interacted with the magnetopause, and then they were

438 partially trapped thereby penetrating into the magnetosphere (Dmitriev and Suvorova, 2015).
439 The amount of this penetrated plasma estimated by the authors can be comparable with estimates
440 of the total amount of plasma entering the dayside magnetosphere (Sibeck, 1999).

441 During the last time period 1658 - 1728 UT shown in panels (a3-g3), we have an excellent
442 opportunity to examine plasma parameters in the magnetosheath region adjacent to the
443 magnetopause. Panels (a3-f3) show two cases of magnetopause distortions followed by short
444 intervals of the magnetosheath from ~1700 to 1701 UT and from 1711 to ~1715 UT. The ULF
445 wave activity is also clearly seen in the magnetic measurement of the TH-E probe (panel g3).
446 The TH-D probe at distance of ~10.8 Re and ~13 LT suddenly crossed the magnetopause and
447 moved into the magnetosheath, a region where the magnetic field vector rotated to negative Bz
448 (panel f3). Plasma in both magnetosheath intervals has extremely high density ($\sim 20 \text{ cm}^{-3}$) and
449 high velocity ($\leq 200 \text{ km/s}$). In the magnetosheath, one can see local pressure pulses around
450 ~1700 UT and ~1712 UT (lines #8 and 9). For #9 case, TH-E observed a small shallow hump of
451 the magnetic field of a few nT between two depletions at 1707 and 1715 UT (panel g3). The last
452 event (#10) shown in Figure 8c is a short penetration of magnetosheath plasma accompanied by
453 a small perturbation in the magnetospheric field observed at ~1724-1725 UT (panels e3, f3).
454 Density and pressure of this structure did not exceed the solar wind parameters, though the
455 velocity was large ($\sim 150 \text{ km/s}$) with dominant negative Vz component (panel b3-d3).

456 Thus, we found typical characteristics of dense and fast plasma jets in all intrusions of the
457 magnetosheath plasma into the magnetosphere and in the magnetosheath itself. Most of these
458 structures caused local compression effects at the dayside. Also, the TH-E magnetic field is
459 modulated by ULF waves in the range of magnetic pulsations Pc 3-4 with period between 10 and
460 60 seconds. As known, dayside Pc 3-4 waves are originated in the upstream solar wind and
461 penetrate into the magnetosphere, while their amplitude is controlled by a foreshock position or
462 IMF orientation (e.g., Guglielmi, 1974).

463 As shown in Figure 3, moderate auroral and polar cap activity was observed during the same
464 time (1600-1800 UT). However, it should be noted that in the preceded interval 1300-1600 UT,
465 associated with the deep electron injections and FEE enhancements, the THEMIS probes also
466 observed similar magnetic compression-expansion effects at inner part of orbits ($\sim 7 - 10 R_e$). At
467 that time, we found enhanced magnetic activity in the polar cap (only in the northern
468 hemisphere), but no auroral activity. This raises an interesting question about spatial pattern of
469 geomagnetic field response to the impact of magnetosheath pressure pulses/plasma jets
470 interacting probably with the dayside magnetopause in the earlier interval 1300-1600 UT with
471 magnetic enhancements #1- #3.

472

473 **2.6. Global ground-based magnetic variations**

474 The global dynamics of geomagnetic field perturbations was studied using 1-min magnetic data
475 provided by an INTERMAGNET of ground magnetometers ([http://www.intermagnet.org/index-
476 eng.php](http://www.intermagnet.org/index-eng.php)). Since there were no pressure pulses in the upstream solar wind and auroral activity was
477 low (see Figure 3), we expect that variations in the geomagnetic field (if any) should result from
478 the local magnetosheath pressure pulses. We used magnetic stations located at geomagnetic
479 latitudes below $\sim 60^\circ$ (Table 3), where a significant effect of different propagation time of
480 magnetohydrodynamic (MHD) waves in the magnetosphere will be almost hidden at 1 min
481 resolution. We grouped magnetic stations in meridional and latitudinal chains.

482 Figure 9 presents relative variations of horizontal (H) component, which was measured at
483 equatorial and low latitudes ranging from 0° to $\sim 20^\circ$ of geomagnetic latitude in the interval from
484 1100 to 1600 UT. In Figure 9, the stations are arranged in local time from morning to
485 postmidnight. The THEMIS magnetic field measurements are also shown at bottom. Four
486 magnetic field pulses of different amplitudes are seen around ~ 1200 , $\sim 1335-1345$, $\sim 1422-1430$
487 and $\sim 1545-1550$ UT practically at all stations. The last three pulses correspond to those observed
488 by THEMIS at ~ 1334 , ~ 1421 and $1547-1550$ UT (#1 - #3, see also Table 2). Moreover, one can

489 see the same pattern of magnetic variation “enhancement and decrease” in both ground-based
490 and satellite observations. Note that the first magnetic pulse at ~1200 UT can not be emerged
491 from THEMIS data because of the large background magnetic field in the inner magnetosphere.
492 Magnetic records at daytime and nighttime are clearly distinguished by amplitudes and time
493 delay relatively to the THEMIS data.

494 Magnetic records at nighttime stations (PHU, GZH, KNY, KDU, GUA, HON, PPT) are
495 characterized by prominent variations of H component, with peak-to peak amplitudes of 3 - 5 nT.
496 The dayside stations (KOU, VSS, MBO, ASC, TSU, BNG, AAE, ABG) show relative weak, but
497 still distinguished, magnetic humps. Smaller amplitude at daytime is a result of an amplifying
498 integral effect from the Chapman-Ferraro current at the magnetopause and ionospheric Sq-
499 current at the ground.

500 It is interesting, that the magnetic pulse at 1200 UT is simultaneously (within the accuracy of ~1
501 min resolution) observed in all local time sectors. However, the other three enhancements were
502 observed in different LT sectors at slightly different time. A time difference varies from ~2 min
503 to ~10 min. The time delay depends on the time moment when a jet interacts with the
504 magnetopause in a given latitude-longitude sector (Dmitriev and Suvorova, 2012).

505 We draw attention to the fact that low-latitude HON and PPT stations, which were located in the
506 predawn sector (2-5 LT) from 1300 to 1500 UT, demonstrate the best coincidence (with a delay
507 of ~1 min) of magnetic enhancements #1 and #2 with those observed by THEMIS near noon.
508 Nighttime and daytime stations (PHU, GZH, KNY, KDU, GUA, MBO, ASC, TSU, BNG, AAE,
509 ABG) observed these peaks with ~3 - 5 min delay. The longest delay (~7 min) for pulses #1 and
510 #2 is found at morning/prenoon stations KOU and VSS (~9 - 11 LT).

511 As we have showed above, the FEE injections (F1 - F6 in Table 1) occur from ~2 to 5 LT. So,
512 we present meridional chains of stations in the predawn and midnight sectors (Figure 10). All
513 magnetic enhancements are well recognized from 0° to 60° of geomagnetic latitude. In midnight
514 and predawn sectors, the first magnetic pulse at ~1200 UT was observed practically

515 simultaneously everywhere. Magnetic pulse #1 around ~1333 UT was delayed by ~7 min at
516 midlatitudes (30° - 60°) in the midnight sector (left panel) and by ~5 min in the predawn sector
517 (right panel). The pulse #2 shows a smaller delay (~3 min) at midlatitudes. The magnetic pulse
518 #3 at most stations in both sectors is observed around ~1545 UT, that is 2 min earlier than at TH-
519 E and 1 min later than at GOES (see Table 2). Thus, the low and middle latitude geomagnetic
520 observations in all local time sectors demonstrate that the magnetic variations of “enhancement-
521 decrease” pattern at 1200-1600 UT were observed by ground magnetometers as a global
522 phenomenon.

523

524 **3. Discussion and Summary**

525 In this work, using NOAA/POES and THEMIS satellites we investigated an unusual case of
526 deep injections of >30 keV electrons at $L < 1.2$ and associated FEE enhancements occurred
527 during quiet, nonstorm condition on August 1, 2008. A series of [postmidnight/predawn](#)
528 injections of >30 keV electrons could be associated with transient magnetospheric magnetic field
529 perturbations. These magnetic perturbations were observed globally like “compression-
530 expansion” effects by THEMIS and GOES 12 in the magnetosphere and by most of ground-
531 based magnetometers from INTERMAGNET network. Comparative analysis of the THEMIS,
532 OMNI and ACE data showed that the magnetic perturbations were caused by impact on the
533 magnetopause by a series of plasma pressure pulses, [so-called jets](#), propagated through the
534 magnetosheath but not in the undisturbed upstream solar wind. Such plasma jets are typical
535 consequence of the foreshock dynamics driven by variations in the IMF orientation (e.g., Lin et
536 al., 1996) and are comprehensively studied using THEMIS and MMS missions (e.g., Archer et
537 al., 2012; 2013; Dmitriev and Suvorova, 2012; 2015; Plaschke et al., 2017). For our case,
538 THEMIS measurements in the region in front of the bow shock, showed obvious evidences of
539 transient quasi-parallel bow shock and foreshock conditions during the interval.

540 The strong FEE enhancements with intensity of [up to \$\sim 10^5\$ \(cm² s sr\)⁻¹](#) were observed by POES
541 above central and eastern Pacific for a long time from ~ 1300 to 2300 UT. With analysis of
542 longitudinal and local time distributions of the enhancements we identified a series of [nightside](#)
543 injections occurred in the sector of $2 - 5$ LT during the period from ~ 1300 to ~ 1700 UT (Figure
544 2). We found that [the first 6 injections](#) (Table 1) occurred before intensification of auroral
545 activity at $1600 - 1800$ UT, and hence, cannot be related to the substorm. [Two](#) injections
546 occurred during the interval of weak auroral activity.

547 The quiet geomagnetic conditions in the period of $1300 - 1600$ UT are consistent with
548 undisturbed solar wind conditions, [which can be](#) obtained from the OMNI data and ACE
549 upstream monitor. However, the picture, emerged from the THEMIS-C magnetic observations
550 right upstream of the subsolar bow shock, showed an apparent discrepancy with OMNI in the
551 magnetic field structures (see Figure 5). For our case, the discrepancy appeared to be due to an
552 inability to predict accurately the evolution of small-scaled structures ([e.g., Zastenker et al., 2000;](#)
553 [Borovsky, 2008](#)), [especially](#) with quasi-radial magnetic tubes, during the propagation to the
554 Earth, and, as result, a notable uncertainty in the time lag method applied in the OMNI database.
555 Erroneous time lag is typical for cases of the quasi-radial IMF orientation (e.g., Case and Wild,
556 2012; Mailyan et al., 2008; [McPherron et al., 2013](#); Bier et al., 2014; Suvorova and Dmitriev,
557 2016). [At worst, THEMIS-C observed magnetic field structures different from those in OMNI](#)
558 [\(as example see Figure 5\)](#). The actual solar wind parameters affecting the magnetosphere were
559 [related](#) to a subsolar foreshock. The analysis of the THEMIS observations helps us to recognize
560 possible external drivers, which might be responsible for the deep FEE injections.

561 During the period $1200 - 1800$ UT, the magnetosphere was periodically under the quasi-radial
562 IMF conditions (Figure 5). During that time, THEMIS-C observed intense ULF activity in the
563 foreshock region. It is well known that the foreshock is also accompanied by ULF waves
564 observed inside the magnetosphere by satellites and ground based magnetometers (e.g.,
565 Guglielmi, 1974; Clausen et al., 2009; Bier et al., 2014). [We study the geomagnetic response](#)

566 with using THEMIS (D, E), GOES-12 geosynchronous satellite, and INTERMAGNET network
567 of ground-base magnetometers. We find that the magnetospheric ULF waves are not strong
568 enough to produce anomalous radial transport of energetic electrons at $L < 1.2$.

569 The THEMIS and GOES measurements clearly show several local effects of magnetosphere
570 compression and expansion in the interval 1200 - 1600 UT (#1 - #3 in Table 2). Similar
571 signatures were found in the H component at majority of ground stations (Figures 9 and 10).
572 Though the geomagnetic response was global, the magnetic pulses were observed first at low
573 latitudes in the postmidnight/predawn sector (2-5 LT). The amplitude of geomagnetic pulses is
574 not very high: from few nT at ground to a few tens of nT at THEMIS. It should be noted that
575 such magnetic perturbations are too weak to produce deep injections of >30 keV electrons below
576 the radiation belt.

577 Analysis of the later interval 1600 - 1800 UT (Figure 7) indicated a possible cause of the
578 magnetic variations (peaks #4 - #10 in Table 2). During that time, THEMIS (D, E) observed
579 magnetic pulses, some of which were accompanied by penetrations of magnetosheath plasma
580 into the magnetosphere. THEMIS also encountered the magnetosheath for a few minutes. We
581 have found that the properties of magnetosheath plasma structures correspond well to high-speed
582 plasma jets [Dmitriev and Suvorova et al., 2012]. The interaction of jets with the magnetopause
583 results in geomagnetic pulses and penetration of the magnetosheath plasma inside the
584 magnetosphere (Figure 8).

585 Note that the upstream conditions observed by THEMIS-C during both time intervals (from 12
586 to 16 UT and from 16 to 18 UT) were similar in that the quasi-radial IMF appeared. Hence, it is
587 reasonable to suggest that the geomagnetic pulses occurred from 12 to 16 UT were also produced
588 by jets because there were no strong enhancements in the solar wind dynamic pressure P_d .
589 Indeed, as one can see in Figures 3 and 8, tenuous variations of P_d do not exceed a few tenths of
590 nPa and, thus, they cannot produce sharp geomagnetic pulses with amplitudes of ~ 10 nT.

591 The magnetosheath pressure pulses or plasma jets arose during time intervals when quasi-radial
592 IMF tubes were passing the subsolar bow shock region as observed by THEMIS. The foreshock
593 was occasionally moving in or out of the subsolar region (see Figure 5). As the spacecraft
594 crossed an interface between two flux tubes, it observed a rotation discontinuity. Passages of the
595 rotational discontinuities followed by change between quasi-parallel and quasi-perpendicular
596 bow shock regimes created favorable conditions for generation of plasma jets (Lin et al., 1996).
597 Note that jets can be generated by directional discontinuities in absence of foreshock conditions
598 (cases #1 and #5) (Dmitriev and Suvorova 2012). THEMIS was able to observe directly such
599 plasma jets in the magnetosheath at later time, when it approached closely the magnetopause.
600 Similar effects of transient magnetospheric compression and expansion and their signatures at
601 low-latitude ground magnetometers were studied by Dmitriev and Suvorova (2012, 2015). As
602 they established, such magnetic field perturbations were caused by magnetosheath plasma jets
603 striking the dayside magnetopause during a foreshock transition through the subsolar region
604 toward flank.

605 Another important effect is penetration of the magnetosheath plasma into the [dayside](#)
606 magnetosphere due to interaction of large-scale jets with the magnetopause (Dmitriev and
607 Suvorova, 2015). Recently, it was revealed that the magnetosheath high-speed jets result in
608 auroral brightening on the dayside (Han et al., 2017; Wang et al., 2018). Sometimes, the dayside
609 aurora penetrates to lower [geomagnetic latitudes of \$\sim 72^\circ\$ from the discrete aurora oval at](#)
610 [geomagnetic latitude \$\sim 76^\circ\$](#) , so-called throat aurora. Han et al. (2017) found that quasi-radial IMF
611 or subsolar foreshock condition is favorable for occurrence of dayside throat aurora, whereas
612 southward IMF has a weaker influence on its occurrence. Based on the comprehensive study of
613 properties of throat aurora, Han et al. (2018) concluded that throat auroras are definite ground
614 signatures for local magnetopause deformations and compressions produced by magnetosheath
615 plasma jet impact. Han et al. (2016) provided direct evidence that the source of precipitating
616 particles in the throat auroras was the magnetosheath plasma (sometimes mixed with

617 magnetospheric plasma), which can be effectively transported by jets from the magnetosheath
618 (e.g., Han et al., 2018). Thus, the jet impact is responsible for generating throat aurora, which
619 provides enhancements in auroral ionospheric conductivity on the dayside.

620 The energy fluxes of hot plasma (from 50 eV to 10 keV) are measured by POES/TED plasma
621 spectrometer. We conducted an additional analysis of hot plasma precipitations in the auroral
622 region at L -shells from 7 to 15 during time interval from 11 to 18 UT on 1 August 2008. Figure
623 11 demonstrates magnetic observations by THEMIS-D and GOES-12, the energy fluxes of
624 auroral precipitations, and FEE injections. We consider intense precipitations with the threshold
625 of $0.5 \text{ (erg cm}^{-2} \text{ s}^{-1}\text{)}$, which is several times higher than the background. One can see that from 11
626 to 16 UT, the hot plasma precipitates mainly on the dayside (12 – 16 LT) while after 16 UT, the
627 precipitations occur practically at all local times both on the day and night sides.

628 The first FEE injection (F1) at ~1250 UT was preceded by several geomagnetic pulses observed
629 by GOES-12. The pulses were not very prominent because at that time, GOES-12 was located in
630 the morning sector. One can see that some of pulses were accompanied by dayside auroral
631 precipitations of the hot plasma. Note that POES satellites have 100 min orbital period and,
632 hence, they can miss some of localized precipitations. On the other hand, when a jet hits the
633 magnetopause, the magnetosheath plasma is not necessarily penetrating into the dayside
634 magnetosphere and, hence, precipitating at high latitudes [*Dmitriev and Suvorova, 2015*].
635 Nevertheless, in Figure 11, we find two cases of geomagnetic pulses followed by intense dayside
636 precipitations of the hot plasma at 1105 UT and 1144 UT.

637 Energetic electrons take a certain time dT to drift from the inner radiation belt edge (at L -shell L_1
638 = 1.2) to the heights of ~900 km (L -shell $L_2 = 1.1\sim 1.15$):

$$639 \quad dT(\text{s}) = 6380 * (L_1 - L_2) / V_{DE} \quad (1)$$

640 where the $E \times B$ drift velocity is determined as

$$641 \quad V_{DE} = 0.032 * L^3 * E, \quad (2)$$

642 where L the average L-shell in the first approach and E is azimuthal electric field in mV/m. From
643 equations (1) and (2), we estimate that the earthward drift of energetic electron across the
644 magnetic field lines from $L = 1.2$ to $L = 1.1$ takes up to 40 min under local electric field of ~ 5
645 mV/m. Note that $E \sim 5$ mV/m was obtained in simulations of energetic electron injections at $L <$
646 1.3 [Selesnick et al., 2016].

647 In our case of non-storm conditions, it is hard to imagine that the strong azimuthal E can persist
648 for so long time. Previously, simulations by Su et al. (2016) have showed that it is not necessary
649 for electrons to be transported earthward all the way during a single injection. Hence, we can
650 consider a multi-step radial transport produced by a number of short pulses of E . In this case, the
651 drift from $L=1.2$ to $L=1.1$ requires two or more pulses of ~ 10 min duration that is comparable
652 with the duration of jet-related disturbances. The multi-step process is limited by the time, during
653 which a particle stays in the region of injection. The >30 keV electrons have a long period of
654 azimuthal drift and, thus, they can stay in the region for hours. In contrast, the >100 keV
655 electrons with the azimuthal period of ~ 6 h leave quickly the injection region and, thus, do not
656 have enough time to penetrate to the forbidden zone. This effect can explain the absence of high-
657 energy electrons in the FEE enhancements presented.

658 We can suggest that the first FEE injection required a long time (\sim hour and longer) and several
659 pulses of E in order to transport energetic electrons from undisturbed edge of the inner radiation
660 belt to $L \sim 1.1$. Then, >30 keV electrons populate L-shells from 1.15 to 1.1 that makes possible to
661 transport electrons to 900 km heights for a short time of ~ 10 min by one pulse of strong E . The
662 latter pattern is applicable for the FEE injection F2 and others. As one can see in Figure 11, each
663 FEE injection after 13 UT is preceded within <30 min by intense auroral precipitations of the hot
664 plasma. The latter is accompanied with geomagnetic pulses produced by the interaction of jets
665 with the magnetopause. It is important to remind that tenuous variations of the solar wind
666 dynamic pressure could not produce the geomagnetic perturbations occurred during the interval
667 considered.

668 We associate the dayside precipitations at high latitudes with the effect of jets piercing the
669 magnetopause. The jets provide penetration of hot plasma from the magnetosheath to the
670 magnetosphere. Dmitriev and Suvorova (2015) have found that the average rate of jet-related
671 penetration of the magnetosheath plasma into the magnetosphere is about 10^{29} particles per day.
672 The penetrated hot ions move quickly (within a few minutes) along the magnetic field lines to
673 high-latitude regions of the dayside ionosphere. We can estimate the flux of precipitating ions of
674 $\sim 10^7$ to 10^8 ($\text{cm}^2 \text{ s}^{-1}$) if we assume that particles precipitate on the dayside arc of 3° width at 70°
675 latitude. This particle flux corresponds well to the energy fluxes of precipitating ions ($>0.5 \text{ erg}$
676 $\text{cm}^{-2} \text{ s}^{-1}$) measured by POES/TED at high latitudes (see Figure 11). Hence, the jet-related
677 magnetosheath plasma can produce significant additional ionization and increase conductivity of
678 the high-latitude ionosphere on the dayside. An enhancement of electric currents in the dayside
679 ionosphere should induce an enhancement of the electric field on the nightside and especially in
680 the predawn sector, where the conductivity is weak. The nightside electric field might penetrate
681 from high to low latitudes and produce ExB drift of electrons from the inner radiation belt to
682 lower heights.

683 Thus, we can propose a scenario when magnetosheath plasma jets, associated with dynamical
684 subsolar foreshock and rotational discontinuities, interact with the dayside magnetopause and
685 cause compression effect with magnetic field perturbations and effective transport of the
686 magnetosheath plasma inside the magnetosphere. The magnetosheath plasma or mix with
687 magnetospheric plasma precipitates to the dayside ionosphere at high latitudes that result in a
688 local increase of the ionospheric conductivity. This in turn promotes generation of transient
689 localized electric fields, which are able to penetrate from high latitudes to very low latitudes (low
690 L-shells). Most favorable conditions for penetration of localized electric fields and FEE
691 enhancements arise in the period from May to September independently on geomagnetic activity
692 level (Suvorova, 2017). Our case event on 1 August 2008 corresponds well to these favorable
693 conditions.

694 Anomalous transport and loss of energetic particles in the magnetosphere was studied and
695 modeled in numerous papers (e.g., Glocer et al., 2011; Selesnick et al., 2016; Su et al., 2016;
696 Turner et al., 2015; Turner et al., 2017a; Zhao and Li, 2013; Zhao et al., 2017a). In the present
697 case, the magnetosphere is driven rather by plasma jets generated locally in the magnetosheath.
698 Moreover, we show that the solar wind conditions right upstream of the bow shock can be
699 substantially different from those measured in the far upstream regions. Another serious problem
700 is the generation/penetration of electric fields in the inner magnetosphere, which is far from
701 complete understanding. Numerical estimations show that the anomalous (fast) radial transport
702 of particles observed in the inner magnetosphere can be produced by the electric field up to 5
703 mV/m (Selesnick et al., 2016; Suvorova et al., 2013). At the present time, there are no models
704 predicting strong electric fields in the inner radiation belt and below. In this sense the scenarios
705 suggested here requires further development of new advanced models of the magnetosheath –
706 magnetosphere – ionosphere coupling.

Acknowledgements

The authors thanks a team of NOAA's Polar Orbiting Environmental Satellites for providing experimental data about energetic particles, the CDAWEB for providing the ACE solar wind data and Kyoto World Data Center for Geomagnetism (<http://wdc.kugi.kyoto-u.ac.jp/index.html>) for providing the geomagnetic indices. We thank the THEMIS team for magnetic and plasma data provided. The results presented in this paper rely on data collected at magnetic observatories. We thank the national institutes that support them and INTERMAGNET for promoting high standards of magnetic observatory practice (www.intermagnet.org). The OMNI data are provided by the GSFC/SPDF OMNIWeb platform (<http://cdaweb.gsfc.nasa.gov/>). The work was supported by grant MOST 106-2811-M-008-050 and MOST 106-2111-M-008-030-MY3 to National Central University.

References

- Archer, M. O., Horbury, T. S., and Eastwood, J. P.: Magnetosheath pressure pulses: Generation downstream of the bow shock from solar wind discontinuities, *J. Geophys. Res.*, 117, A05228, <https://doi.org/10.1029/2011JA017468>, 2012.
- Archer, M. O., Horbury, T. S., Eastwood, J. P., Weygand, J. M., and Yeoman, T. K.: Magnetospheric response to magnetosheath pressure pulses: A low-pass filter effect, *J. Geophys. Res.*, 118, 5454-5466, <https://doi.org/10.1002/jgra.50519>, 2013.

- Asikainen, T., and Mursula, K.: Filling the South Atlantic anomaly by energetic electrons during a great magnetic storm, *Geophys. Res. Lett.*, 32, L16102, <https://doi.org/10.1029/2005GL023634>, 2005.
- Auster, H. U., Glassmeier, K. H., Magnes, W., Aydogar, O., Baumjohann, W., Constantinescu, D., Fischer, D., Fornacon, K. H., Georgescu, E., Harvey, P., Hillenmaier, O., Kroth, R., Ludlam, M., Narita, Y., Nakamura, R., Okrafka, K., Plaschke, F., Richter, I., Schwarzl, H., Stoll, B., Valavanoglou, A., Wiedemann, M.: The THEMIS fluxgate magnetometer, *Space Sci. Rev.*, 141(1–4), 235–264, <https://doi.org/10.1007/s11214-008-9365-9>, 2008.
- Bier, E. A., Owusu, N., Engebretson, M. J., Posch, J. L., Lessard, M. R., and Pilipenko V. A.: Investigating the IMF cone angle control of Pc3-4 pulsations observed on the ground, *J. Geophys. Res. Space Physics*, 119, 1797-1813, <https://doi.org/10.1002/2013JA019637>, 2014.
- Borovsky, J. E.: Flux tube texture of the solar wind: Strands of the magnetic carpet at 1 AU? *J. Geophys. Res.*, 113, A08110, <https://doi.org/10.1029/2007JA012684>, 2008.
- Case, N. A., and Wild, J. A.: A statistical comparison of solar wind propagation delays derived from multispacecraft techniques, *J. Geophys. Res.*, 117, A02101, <https://doi.org/10.1029/2011JA016946>, 2012.
- Clausen, L. B. N., Yeoman, T. K., Fear, R. C., Behlke, R., Lucek, E. A., and Engebretson, M. J.: First simultaneous measurements of waves generated at the bow shock in the solar wind, the magnetosphere and on the ground, *Annales Geophysicae*, 27, 357-371, <https://doi.org/10.5194/angeo-27-357-2009>, 2009.
- Crooker, N. U., Eastman, T. E., Frank, L. A., Smith, E. J., and Russell, C. T.: Energetic magnetosheath ions and the interplanetary magnetic field orientation, *J. Geophys. Res.*, 86, 4455-4460, 1981.
- Dmitriev, A. V., and Suvorova, A. V.: Traveling magnetopause distortion related to a large-scale magnetosheath plasma jet: THEMIS and ground-based observations, *J. Geophys. Res.*, 117, A08217, <https://doi.org/10.1029/2011JA016861>, 2012.
- Dmitriev, A. V., and Suvorova, A. V.: Large-scale jets in the magnetosheath and plasma penetration across the magnetopause: THEMIS observations, *J. Geophys. Res. Space Physics*, 120, 4423–4437, <https://doi.org/10.1002/2014JA020953>, 2015.
- Dmitriev, A. V., and Yeh, H.-C.: Storm-time ionization enhancements at the topside low-latitude ionosphere, *Ann. Geophys.*, 26, 867-876, 2008.
- Dmitriev, A. V., Suvorova, A. V., Klimenko, M. V., Klimenko, V. V., Ratovsky, K. G., Rakhmatulin, R. A., and Parkhomov, V. A.: Predictable and unpredictable ionospheric disturbances during St. Patrick's Day magnetic storms of 2013 and 2015 and on 8-9 March 2008, *J. Geophys. Res.: Space Physics*, 122, 2398-2432, <https://doi.org/10.1002/2016JA023260>, (2017).
- Glocer, A., Fok, M.-C., Nagai, T., Tóth, G., Guild, T., and Blake, J.: Rapid rebuilding of the outer radiation belt, *J. Geophys. Res.*, 116, A09213, <https://doi.org/10.1029/2011JA016516>, 2011.
- Gosling, J. T., Asbridge, J. R., Bame, S. J., Paschmann, G., and Sckopke, N.: Observations of two distinct populations of bow shock ions in the upstream solar wind, *J. Geophys. Res.*, 5, 957–960, 1978.
- Greenstadt, E. W., Russell, C. T., and Hoppe, M.: Magnetic field orientation and suprathermal ion streams in the earth's foreshock, *J. Geophys. Res.*, 85, 3473–3479, 1980.
- Guglielmi, A.: Diagnostics of the magnetosphere and interplanetary medium by means of pulsations, *Space Sci. Rev.*, 16(3), 331–345, 1974.

- Evans, D. S.: Dramatic increases in the flux of >30 keV electrons at very low L-values in the onset of large geomagnetic storms, *EOS Trans.*, 69(44), 1393, 1988.
- Evans, D. S., and Greer, M. S.: Polar Orbiting Environmental Satellite Space Environment Monitor: 2. Instrument descriptions and archive data documentation. Tech. Memo. version 1.4, NOAA Space Environ. Lab., Boulder, Colo., 2004.
- Heikkila, W. J.: Soft particle fluxes near the equator, *J. Geophys. Res.*, 76, 1076-1078, 1971.
- Han, D.-S., Nishimura, Y., Lyons, L. R., Hu, H.Q., and Yang, H. G.: Throat aurora: The ionospheric signature of magnetosheath particles penetrating into the magnetosphere, *Geophysical Research Letters*, 43, 1819-1827, <https://doi.org/10.1002/2016GL068181>, 2016.
- Han, D.-S., Hietala, H., Chen, X.-C., Nishimura, Y., Lyons R. L., Liu, J.-J., Hu, H.-Q., and Yang, H.-G.: Observational properties of dayside throat aurora and implications on the possible generation mechanisms, *J. Geophys. Res. Space Physics*, 122, 1853-1870, <https://doi.org/10.1002/2016JA023394>, 2017a.
- Han, D.-S., Liu, J.-J., Chen, X.-C., Xu, T., Li, B., Hu, Z.-J., Hu, H. Q., Yang, H. G., Fuselier, S. A., and Pollock, C.J.: Direct evidence for throat aurora being the ionospheric signature of magnetopause transient and reflecting localized magnetopause indentations. *J. Geophys. Res. Space Physics*, 123, 2658-2667, <https://doi.org/10.1002/2017JA024945>, 2018.
- Imhof, W. L., Gaines, E. E., and Reagan, J. B.: Dynamic variations in intensity and energy spectra of electrons in the inner radiation belt. *J. Geophys. Res.*, 78(22), 4568–4577, 1973a.
- Kikuchi, T. and Evans, D.S.: Energetic electrons observed by NOAA-6 over Japan (L=1.3) at the time of geomagnetic storm on February 8-9, 1986, *Proc. Res. Inst. Atmos., Nagoya University*, 36, 137-150, 1989.
- King, J. H., and Papitashvili, N. E.: Solar wind spatial scales in and comparisons of hourly Wind and ACE plasma and magnetic field data, *J. Geophys. Res.*, 110, A02104, <https://doi.org/10.1029/2004JA010649>, 2005.
- Krasovskii, V. I., Shklovski, I. S., Galperin, Yu. I., Svetlitskii, E. M., Kushnir, Yu. M., and Bordovskii, G. A.: The detection of electrons with energies of approximately 10 keV in the upper atmosphere (in Russian). *Iskusstvennye Sputniki Zemli*, 6, 113-126, (English translation: *Planet. Space Sci.*, 9, 27-40, 1962), 1961.
- Lejosne, S., and Mozer, F. S.: Typical values of the electric drift $E \times B/B^2$ in the inner radiation belt and slot region as determined from Van Allen Probe measurements, *J. Geophys. Res. Space Physics*, 121, 12,014–12,024, <https://doi.org/10.1002/2016JA023613>, 2016.
- Lin, Y., Lee, L. C., and Yan, M.: Generation of dynamic pressure pulses downstream of the bow shock by variations in the interplanetary magnetic field orientation, *J. Geophys. Res.*, 101, 479–493, 1996.
- Lin, R. L., Zhang, X. X., Liu, S. Q., Wang, Y. L., and Gong, J. C.: A three-dimensional asymmetric magnetopause model. *J. Geophys. Res.*, 115, A04207, <https://doi.org/10.1029/2009JA014235>, 2010.
- Mailyan, B., Munteanu, C., and Haaland, S.: What is the best method to calculate the solar wind propagation delay? *Ann. Geophys.*, 26, 2383–2394, 2008.
- Matsui, H., Torbert, R. B., Spence, H. E., Khotyaintsev, Yu. V., and Lindqvist, P.-A.: Revision of empirical electric field modeling in the inner magnetosphere using Cluster data, *J. Geophys. Res. Space Physics*, 118, 4119–4134, <https://doi.org/10.1002/jgra.50373>, 2013.
- McFadden, J. P., Carlson, C. W., Larson, D., Ludlam, M., Abiad, R., Elliott, B., Turin, P., Marckwordt, M., and Angelopoulos, V.: The THEMIS ESA plasma instrument and in-flight calibration, *Space Sci. Rev.*, 141, 277–302, <https://doi.org/10.1007/s11214-008-9440-2>, 2008.

- McIlwain, C. E.: Coordinates for mapping the distribution of magnetically trapped particles, *J. Geophys. Res.*, 66, 3681-3691, 1961.
- McPherron, R. L., Baker, D. N., Pulkkinen, T. I., Hsu, T. S., Kissinger, J., and Chu, X.: Changes in solar wind-magnetosphere coupling with solar cycle, season, and time relative to stream interface, *J. Atmos. Sol. Terr. Phys.*, 99, 1-13, <https://doi.org/10.1016/j.jastp.2012.09.003>, 2013.
- Park J., Min, K. W., Summers, D., Hwang, J., Kim, H. J., Horne, R. B., Kirsch, P., Yumoto, K., Uozumi, T., Lühr, H., and Green, J.: Non-stormtime injection of energetic particles into the slot region between Earth's inner and outer electron radiation belts as observed by STSAT-1 and NOAA-POES, *Geophys. Res. Lett.*, 37, L16102, <https://doi.org/10.1029/2010GL043989>, 2010.
- Paschmann, G., Sckopke, N., Bame, N., Gosling, J.T., Russell, C.T., and Greenstadt, E.W.: Association of low-frequency waves with suprathermal ions in the upstream solar wind, *Geophys. Res. Lett.*, 6, 209-212, 1979.
- Paulikas, G. A.: Precipitation of particles at low and middle latitudes, *Rev. Geophys. Space Phys.*, 13(5), 709-734, 1975.
- Pfizer, K. A., and Winckler, J. R.: Experimental observation of a large addition to the electron inner radiation belt after a solar flare event, *J. Geophys. Res.*, 73(17), 5792-5797, 1968.
- Plaschke, F., Karlsson, T., Hietala, H., Archer, M., Voros, Z., Nakamura, R., Magnes, W., Baumjohann, W., Torbert, R. B., Russell, C. T., and Giles, B. L.: Magnetosheath high-speed jets: Internal structure and interaction with ambient plasma, *Journal of Geophysical Research: Space Physics*, 122, 10,157-10,175, 2017.
- Rowland, D. E., and Wygant, J. R.: Dependence of the large-scale, inner magnetospheric electric field on geomagnetic activity, *J. Geophys. Res.*, 103(A7), 14959-24964, 1998.
- Reeves, G. D., Friedel, R. H. W., Larsen, B. A., Skoug, R. M., Funsten, H. O., Claudepierre, S. G., Fennell, J. F., Turner, D. L., Denton, M. H., Spence, H. E., Blake, J. B., and Baker, D.N.: Energy-dependent dynamics of keV to MeV electrons in the inner zone, outer zone, and slot regions, *J. Geophys. Res.*, 121, 397-412, <https://doi.org/10.1002/2015JA021569>, 2016.
- Savenko, I. A., Shavrin, P. I., and Pisarenko, N. F.: Soft particle radiation at an altitude of 320 km in the latitudes near the equator (in russian). *Iskusstvennye Sputniki Zemli*, 13, 75-80 (English translation: *Planet. Space Sci.*, 11, 431-436, 1963), 1962.
- Schwartz, S. J., and Burgess, D.: Quasi-parallel shocks: A patchwork of three-dimensional structures, *Geophys. Res. Lett.*, 18, 373-376, 1991.
- Selesnick, R. S., Su, Y.-J., and Blake, J. B.: Control of the innermost electron radiation belt by large-scale electric fields, *J. Geophys. Res. Space Physics*, 121, 8417-8427, <https://doi.org/10.1002/2016JA022973>, 2016.
- Sibeck, D. G.: Plasma transfer processes at the magnetopause, *Space Sci. Rev.*, 88, 207-283, <https://doi.org/10.1023/a:1005255801425>, 1999.
- Su, Y.-J., Selesnick, R. S., and Blake J. B.: Formation of the inner electron radiation belt by enhanced large-scale electric fields, *J. Geophys. Res. Space Physics*, 121, 8508-8522, <https://doi.org/10.1002/2016JA022881>, 2016.
- Suvorova, A. V., and Dmitriev, A. V.: Radiation aspects of geomagnetic storm impact below the radiation belt, In V. P. Banks (Ed.), *Cyclonic and Geomagnetic Storms: Predicting Factors, Formation and Environmental Impacts*, (pp. 19-75), New York: NOVA Science Publishers, Inc., 2015.
- Suvorova, A. V., and Dmitriev, A. V.: On magnetopause inflation under radial IMF, *Adv. Space Res.*, 58, 249-256, 2016.

- Suvorova, A. V., Dmitriev, A.V., and Tsai, L.-C.: On relation between mid-latitude ionospheric ionization and quasi-trapped energetic electrons during 15 December 2006 magnetic storm, *Planet. Space Sci.*, 60, 363-369, <https://doi.org/10.1016/j.pss.2011.11.001>, 2012.
- Suvorova, A. V., Dmitriev, A. V., Tsai, L.-C., Kunitsyn, V. E., Andreeva, E. S., Nesterov, I. A., and Lazutin, L. L.: TEC evidence for near-equatorial energy deposition by 30 keV electrons in the topside ionosphere, *J. Geophys. Res.*, 118, 4672–4695, <https://doi.org/10.1002/jgra.50439>, 2013.
- Suvorova, A. V., Huang, C.-M., Matsumoto, H., Dmitriev, A. V., Kunitsyn, V. E., Andreeva, E. S., Nesterov, I. A., and Tsai, L.-C.: Low-latitude ionospheric effects of energetic electrons during a recurrent magnetic storm, *J. Geophys. Res. Space Physics*, 119, 9283-9303, <https://doi.org/10.1002/2014JA020349>, 2014.
- Suvorova, A. V., Huang, C.-M., Dmitriev, A. V., Kunitsyn, V. E., Andreeva, E. S., Nesterov, I. A., Klimenko, M. V., Klimenko, V. V., and Tumanova, Yu. S.: Effects of ionizing energetic electrons and plasma transport in the ionosphere during the initial phase of the December 2006 magnetic storm, *J. Geophys Res.: Space Physics*, 121, 5880-5896, <https://doi.org/10.1002/2016JA022622>, 2016.
- Suvorova, A.V.: Flux enhancements of >30 keV electrons at low drift shells $L < 1.2$ during last solar cycles, *J. Geophys Res.: Space Physics*, 122, 12274-12287, <https://doi.org/10.1002/2017JA024556>, 2017.
- Tadokoro, H., Tsuchiya, F., Miyoshi, Y., Misawa, H., Morioka, A., and Evans, D. S.: Electron flux enhancement in the inner radiation belt during moderate magnetic storms, *Ann. Geophys.*, 25, 1359-1364, 2007.
- Tanaka, Y., Nishino, M., and Iwata, A.: Magnetic storm-related energetic electrons and magnetospheric electric fields penetrating into the low-latitude magnetosphere ($L \sim 1.5$), *Planet. Space Sci.*, 38(8), 1051-1059, 1990.
- Troshichev, O. A., Andrezen, V. G., Vennerstrøm, S., and Friis-Christensen, E.: Magnetic activity in the polar cap – A new index, *Planet. Space Sci.*, 36(11), 1095–1102, 1988.
- Turner, D. L., Claudepierre, S. G., Fennell, J. F., O'Brien, T. P., Blake, J. B., Lemon, C., Gkioulidou, M., Takahashi, K., Reeves, G. D., Thaller, S., Breneman, A., Wygant, J. R., Li, W., Runov, A., and Angelopoulos, V.: Energetic electron injections deep into the inner magnetosphere associated with substorm activity, *Geophys. Res. Lett.*, 42, 2079-2087, <https://doi.org/10.1002/2015GL063225>, 2015.
- Turner, D. L., Fennell, J. F., Blake, J. B., Claudepierre, S. G., Clemmons, J. H., Jaynes, A. N., Leonard, T., Baker, D. N., et al.: Multipoint observations of energetic particles injections and substorm activity during a conjunction between Magnetospheric Multiscale (MMS) and Van Allen Probes, *J. Geophys. Res. Space Physics*, 122, 11481-11504, <https://doi.org/10.1002/2017JA024554>, 2017a.
- Turner, D. L., O'Brien, T.P., Fennell, J.F., Claudepierre, S. G., Blake, J. B., Jaynes, A. N., Baker, D. N., Kanekal, S., Gkioulidou, M., Henderson, M. G., and Reeves, G. D.: Investigating the source of near-relativistics and relativistics electrons in Earth's inner radiation belt, *J. Geophys. Res. Space Physics*, 122, 695-710, <https://doi.org/10.1002/2016JA023600>, 2017b.
- Zastenker, G. N., Dalin, P. A., Petrukovich, A. A., et al.: Solar wind structure dynamics by multipoint observations, *Phys. Chem. Earth (C)*, 25 (1-2), 137-140, 2000.
- Zhao, H., and Li, X.: Modeling energetic electron penetration into the slot region and inner radiation belt, *J. Geophys. Res. Space Physics*, 118, 6936-6945, <https://doi.org/10.1002/2013JA019240>, 2013.

- Zhao, H., Li, X., Baker, D.N., Claudepierre, S.G., Fennell, J. F., Blake, J. B., Larsen, B. A., Skoug, R. M., Funsten, H. O., Friedel, R. H. W., Reeves, G. D., Spence, H. E., Mitchell, D. G., and Lanzerotti, L. J.: Ring current electron dynamics during geomagnetic storms based on the Van Allen Probes measurements, *J. Geophys. Res. Space Physics*, 121, 3333-3346, <https://doi.org/10.1002/2016JA022358>, 2016.
- Zhao, H., Baker, D.N., Califf, S., Li, X., Jaynes, A. N., Leonard, T., Kanekal, S. G., Blake, J. B., Fennell, J. F., Claudepierre, S. G., Turner, D. L., Reeves, G. D., and Spence, H. E.: Van Allen Probes measurements of energetic particle deep penetration into the low L region ($L < 4$) during the storm on 8 April 2016, *J. Geophys. Res.*, 122, 12140-12152, <https://doi.org/10.1002/2017JA024558>, 2017a.
- Zhao, H., Baker, D. N., Jaynes, A. N., Li, X., Elkington, S. R., Kanekal, S. G., Spence, H. E., Boyd, A. J., Huang, C.-L., and Forsyth, C.: On the relation between radiation belt electrons and solar wind parameters/geomagnetic indices: Dependence on the first adiabatic invariant and L^* , *J. Geophys. Res. Space Physics*, 122, 1624-1642, <https://doi.org/10.1002/2016JA023658>, 2017b.
- Wang, B., Nishimura, Y., Heitala, H., Lyons, L., Angelopoulos, V., Plaschke, F., Ebihara, Y., and Weatherwax, A.: Impacts of magnetosheath high-speed jets on the magnetosphere and ionosphere measured by optical imaging and satellite observations, *J. Geophys. Res. Space Physics*, 123, 4879-4894, <https://doi.org/10.1002/2017JA024954>, 2018.

Table 1 *FEE Enhancements observed by POES satellites*

FEE ID #	POES s/c ID	Observed time hh:mm UT	Longitude deg	LT* h
F1	P8	12:50	-164.2	1.8
F2	P5	13:15	-128.8	5.1
F3	P6	13:53	-138.3	5.1
F4	P8	14:32	169.7	1.6
F5	P5	14:54	-152.7	5.1
F6	P6	15:34	-162.5	5.0
F7	P2	15:44	-98.7	9.3
F8	P5	16:33	-170.1	5.0
F9	P7	16:37	-107.3	9.7
F10	P6	17:12	180.0	4.9
F11	P2	17:24	-123.0	9.4
F12	P7	18:16	-131.0	9.8
F13	P2	19:06	-140.0	9.6
F14	P8	20:30	-105.0	13.8
F15	P6	23:09	-94.5	17.2

* Local time

Table 2 *Timing of Magnetic Field Enhancements and Plasma Pulses from THEMIS and GOES12*

ID #	s/c ID	Time of magnetic peak hh:mm:ss	Time of pressure pulse hh:mm:ss	Foreshock signatures
1	TH-D	13:33:40		absent
	TH-E	13:33:40		
	TH-B	13:33:40		
	G12	13:35:40		
2	TH-D	14:20:50		ions, ULF
	TH-E	14:20:50		
	TH-B	14:20:50		
	G12	14:20:50		
3	TH-D	15:50:30		ions, ULF
	TH-E	15:47:30		
	G12	15:44:00		
4	TH-D	16:14:05	~16:15 - 16:16	ions, ULF
	TH-E	16:14:05		
5	TH-D	16:38:20	16:40	absent
	TH-E	16:38:40		
6	TH-D	16:47:45	16:47:55	ions
	TH-E	16:47:45		
7	TH-D	-	16:51:22	ions, ULF
	TH-E	-		
8	TH-D	magnetosheath	17:00:25	ions, ULF
	TH-E	-		
9	TH-D	magnetosheath	~17:12 - 17:13	ions
	TH-E	17:12:30		
10	TH-D	17:24:50	17:24:50	ions, ULF
	TH-E	-		

Table 3*Location of Magnetic Stations in Geographic and Geomagnetic coordinates*

Code	Name	GLat ^a	GLon ^a	MLat ^b	MLon ^b
AAE	Addis Ababa	9.0	38.8	5.3	109.9
ABG	Alibag	18.6	72.9	9.5	144.4
ASC	Ascension Island	-8.0	-14.4	-1.4	54.7
ASP	Alice Springs	-23.8	133.9	-34.1	-153.6
BNG	Bangui	4.3	18.6	4.6	89.3
CMO	College	64.9	-147.9	64.8	-102.6
CNB	Canberra	-35.3	149.4	-43.8	-134.5
CTA	Charters Towers	-20.1	146.3	-29.1	-140.7
EYR	Eyrewell	-43.4	172.4	-47.8	-107.0
GUA	Guam	13.6	144.9	4.2	-146.3
GZH	Zhaoqing	23.0	112.5	11.7	-177.1
HON	Honolulu	21.3	-158.0	21.2	-92.7
KAK	Kakioka	36.2	140.2	26.2	-153.3
KDU	Kakadu	-12.7	132.5	-23.2	-156.3
KNY	Kanoya	31.4	130.9	20.7	-161.2
KOU	Kourou	5.2	-52.7	16.1	17.7
MBO	Mbour	14.4	-17.0	21.1	55.8
MCQ	McQuarie Island	-54.5	159.0	-60.9	-116.2
MMB	Memambetsu	43.9	144.2	34.2	-150.9
PET	Paratunka	53.0	158.3	45.6	-138.5
PHU	Phuthuy	21.0	106.0	9.7	176.0
PPT	Pamatai	-17.6	-149.6	-15.2	-76.5
SHU	Shumagin	55.4	199.5	54.1	-103.1
SIT	Sitka	57.1	-135.3	60.1	-83.7
TSU	Tsumeb	-19.2	17.6	-18.3	83.5
VSS	Vassouras	-22.4	-43.7	-12.1	24.6

^a Geographic latitude and longitude^b Magnetic latitude and longitude

FIGURE CAPTIONS

Figure 1. Geographic distribution of >30 keV electron fluxes measured by five NOAA/POES satellites on August 1, 2008 for the time interval (a) 0-12 UT, before the electron flux enhancements and (b) 12-24 UT, during the enhancements. **The electrons are detected in vertical direction. In the forbidden zone those electrons are quasi-trapped.** The electron fluxes enhanced largely during nonstorm condition after 12 UT. The forbidden zone is bounded by $L=1.2$ (white lines) and located outside of the South Atlantic Anomaly (SAA) at equatorial-to-low latitudes. The solid black curve indicates the dip equator.

Figure 2. FEE enhancements on 1 August 2008: (a) fluxes of >30 keV electrons in units $(\text{cm}^2 \text{ s sr})^{-1}$, (b) L-shell of enhancements, (c) longitude and (d) local time of peak fluxes (black circles). Measurements within the SAA area are indicated by the open circles. Colorful curves denote NOAA/POES satellites: P2 (black), P5 (pink), P6 (red), P7 (blue), and P8 (green). **Horizontal dashed line at panel (b) depicts the lower edge of the inner radiation belt. FEE enhancements peak at the equator (minimal L-shells) that indicates a fast radial transport from the inner radiation belt.**

Figure 3. Solar wind parameters from OMNI data and geomagnetic indices on August 1, 2008. From top to bottom: (a) solar wind density (black) and dynamic pressure (blue), (b) solar wind speed, (c) interplanetary magnetic field (IMF) components B_x (blue), B_y (green), B_z (red) and magnitude B (black) in Geocentric Solar Magnetospheric (GSM) coordinates, (d) polar cap magnetic activity index PCN for northern (blue) and PCS for southern (red) hemispheres, (e) auroral electrojet index AE (black), AL (red), AU (green), and (f) storm time ring current variation index SYM-H. The shaded box denotes the time interval from 13 to 23 UT, when the nonstorm FEE enhancements were observed.

Figure 4. Spacecraft positions in GSM coordinates from 1200 to 1800 UT on August 1, 2018. The TH-C probe (blue) was in front of the subsolar bow shock. The TH-E (orange), TH-D (green), TH-B (brown), and GOES 12 (black) were located inside the dayside magnetosphere. The magnetopause position (black curve) was calculated using OMNI data for the upstream conditions at ~ 1600 UT following the model by Lin et al.'s (2010).

Figure 5. Observations of plasma and magnetic field on August 1, 2008. (a) Ion spectrogram (ion flux is in units of $\text{eV}/\text{cm}^2 \text{ s sr eV}$) and IMF vector components in GSM coordinates measured by TH-C, (b) IMF vector components from OMNI data set, (c) IMF cone angles plotted for TH-C (red) and OMNI (black).

Figure 6. Satellite measurements of magnetic field and plasma in the dayside magnetosphere and geomagnetic activity. (a) The Bz-GSM components from THEMIS probes TH-B (brown), TH-E (orange), and TH-D (green). The left y-axis corresponds to the magnetic measurements from TH-B and TH-D, and the right y-axis to TH-E. (b) The magnetic field strength from GOES-12 (black); (c) the SYM-H index; and (d) the ion spectrogram from TH-D (ion flux is in units of $\text{eV}/\text{cm}^2 \text{ s sr eV}$). Dashed lines, numbered from 1 to 10, indicate time moments of magnetic and plasma disturbances observed by THEMIS.

Figure 7. Observations of plasma and magnetic field at 1530-1800 UT on August 1, 2008: (a-c) ion spectrograms measured by TH-C, TH-D, and TH-E (ion flux is in units of $\text{eV}/\text{cm}^2 \text{ s sr eV}$), (d) SYM-H index, (e) AE (black) and AL (red) indices, (f) horizontal magnetic field H_p detected by GOES 12 from 10 to 13 LT, (g) magnetic field strengths B_{tot} from TH-D (green) and TH-E (red), (h) IMF cone angles for TH-C (black) and for the ACE upstream monitor (blue). The ACE measurements are delayed by 60 min. Dashed lines and numbers #4 - #10 mark magnetospheric disturbances with magnetosheath ion population observed in the magnetosphere.

Figure 8. Observations of plasma and magnetic field during the intervals 1600 - 1630 UT, 1630 - 1700 UT and 1658 - 1728 UT on August 1, 2008. Panels show from top to bottom: (a) ion spectrogram from TH-D, (b) total pressure P_{tot} measured by the ACE upstream monitor (black) and TH-D (red), (c) plasma density D measured by ACE (black) and TH-D (blue), (d) TH-D measurements of bulk velocity V (black) and its components in GSM coordinates V_x (blue), V_y (green) and V_z (red), (e) transversal components of magnetic field B_x (blue) and B_y (green) from TH-D, (f) magnitude B and B_z component of magnetic field from TH-D, (g) magnitude B and B_z component of magnetic field from TH-E. The magnetosheath plasma penetration is denoted by dashed lines and numbers #4 - #10.

Figure 9. Relative variations in the horizontal component (H) of the geomagnetic field at low geomagnetic latitudes. Local time intervals are indicated near the station codes. The vertical lines depict time of the magnetic pulses at THEMIS (lines #1 - #3). Bottom panel shows magnetic field B measured by TH-E (orange) and by TH-D (green).

Figure 10. Relative variations in the horizontal component (H) of the geomagnetic field in the midnight (left) and predawn (right) sectors. The geomagnetic latitudes of the stations are indicated near station codes. The vertical lines depict time of the magnetic pulses at THEMIS.

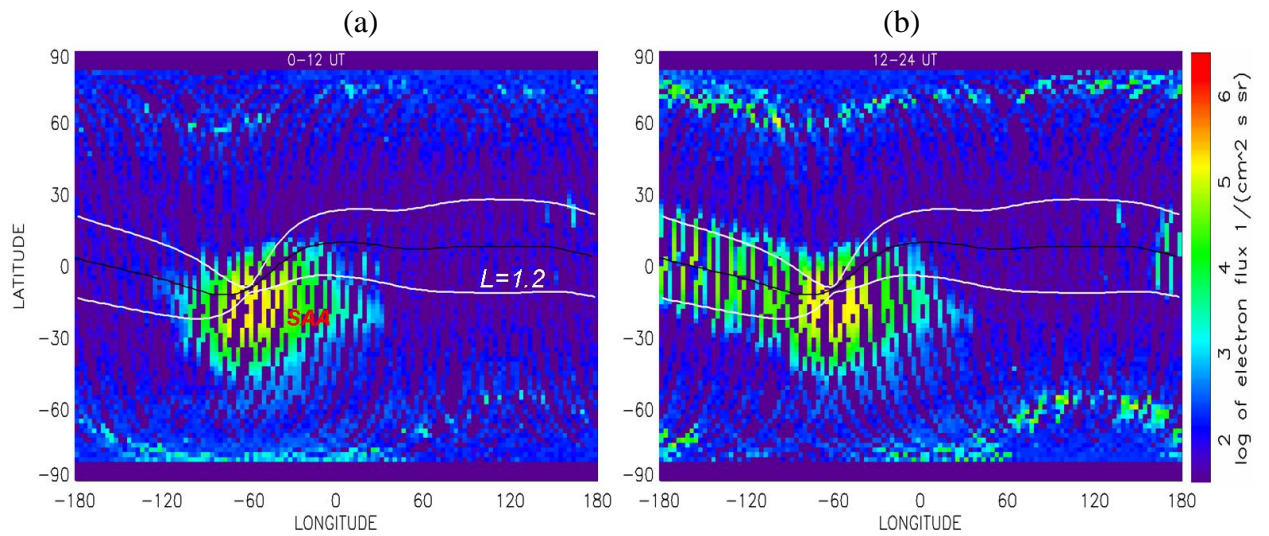


Figure 1. Geographic distribution of >30 keV electron fluxes measured by five NOAA/POES satellites on August 1, 2008 for the time interval (a) 0-12 UT, before the electron flux enhancements and (b) 12-24 UT, during the enhancements. The electrons are detected in vertical direction. In the forbidden zone those electrons are quasi-trapped. The electron fluxes enhanced largely during nonstorm condition after 12 UT. The forbidden zone is bounded by $L=1.2$ (white lines) and located outside of the South Atlantic Anomaly (SAA) at equatorial-to-low latitudes. The solid black curve indicates the dip equator.

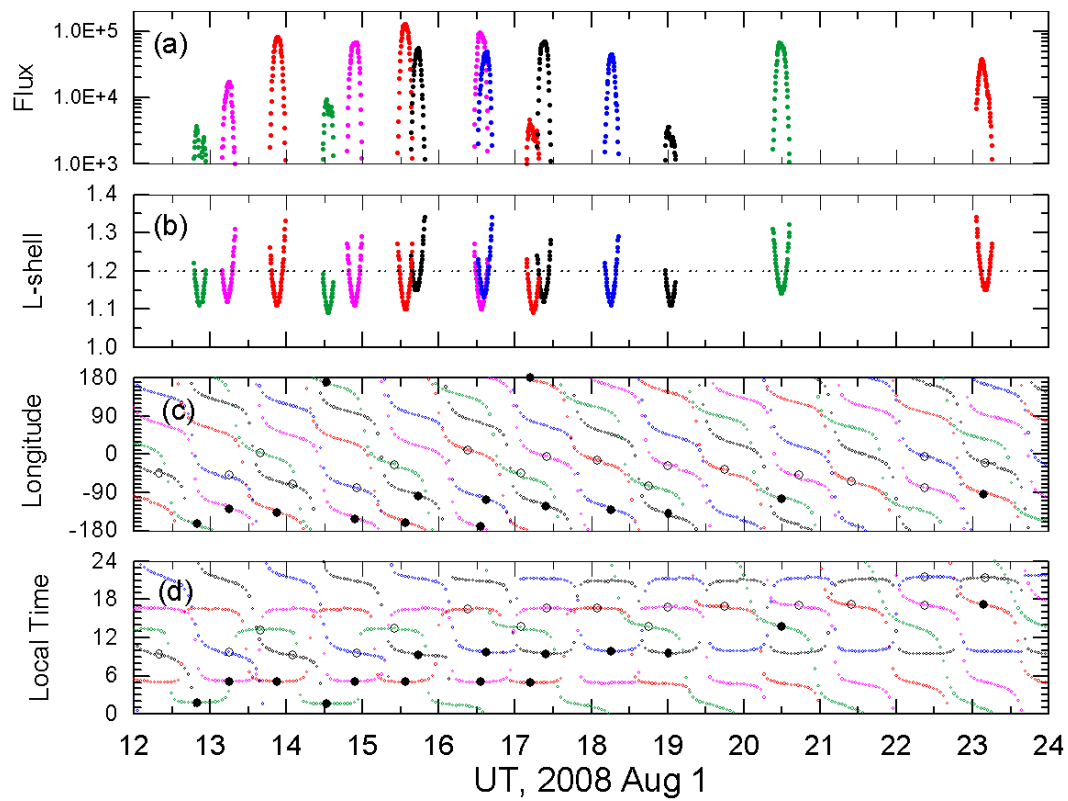


Figure 2. FEE enhancements on 1 August 2008: (a) fluxes of >30 keV electrons in units $(cm^2 s sr)^{-1}$, (b) L-shell of enhancements, (c) longitude and (d) local time of peak fluxes (black circles). Measurements within the SAA area are indicated by the open circles. Colorful curves denote NOAA/POES satellites: P2 (black), P5 (pink), P6 (red), P7 (blue), and P8 (green). Horizontal dashed line at panel (b) depicts the lower edge of the inner radiation belt. FEE enhancements peak at the equator (minimal L-shells) that indicates a fast radial transport from the inner radiation belt.

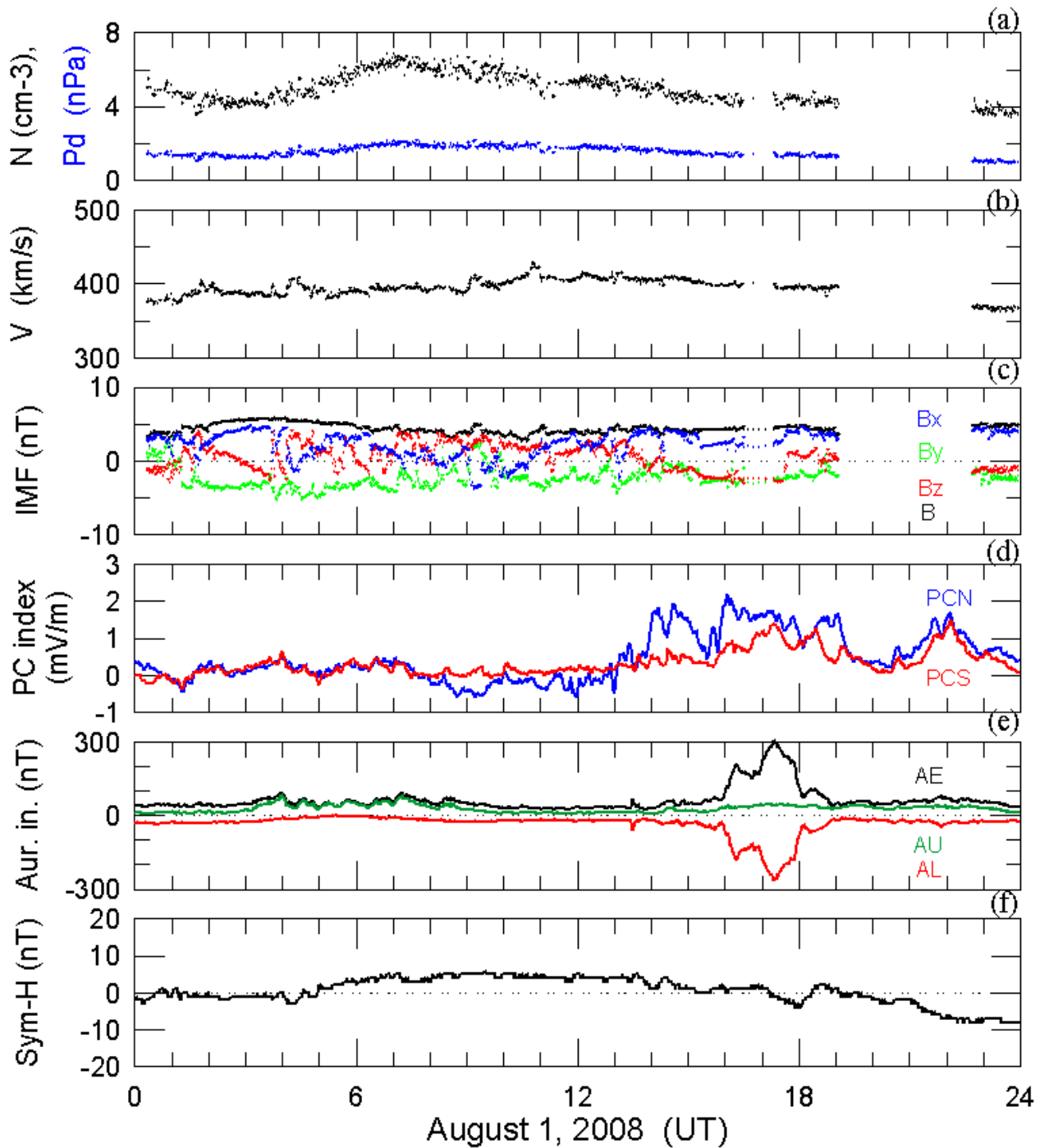


Figure 3. Solar wind parameters from OMNI data and geomagnetic indices on August 1, 2008. From top to bottom: (a) solar wind density (black) and dynamic pressure (blue), (b) solar wind speed, (c) interplanetary magnetic field (IMF) components B_x (blue), B_y (green), B_z (red) and magnitude B (black) in Geocentric Solar Magnetospheric (GSM) coordinates, (d) polar cap magnetic activity index PCN for northern (blue) and PCS for southern (red) hemispheres, (e) auroral electrojet index AE (black), AL (red), AU (green), and (f) storm time ring current variation index SYM-H. The shaded box denotes the time interval from 13 to 23 UT, when the nonstorm FEE enhancements were observed.

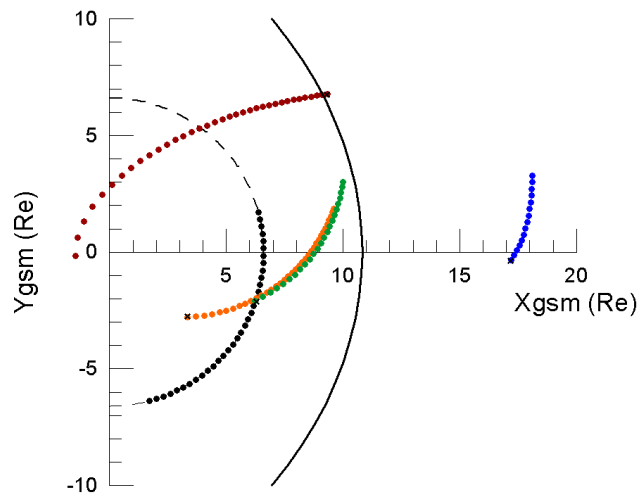


Figure 4. Spacecraft positions in GSM coordinates from 1200 to 1800 UT on August 1, 2018. The TH-C probe (blue) was in front of the subsolar bow shock. The TH-E (orange), TH-D (green), TH-B (brown), and GOES 12 (black) were located inside the dayside magnetosphere. The magnetopause position (black curve) was calculated using OMNI data for the upstream conditions at ~ 1600 UT following the model by Lin et al.'s (2010).

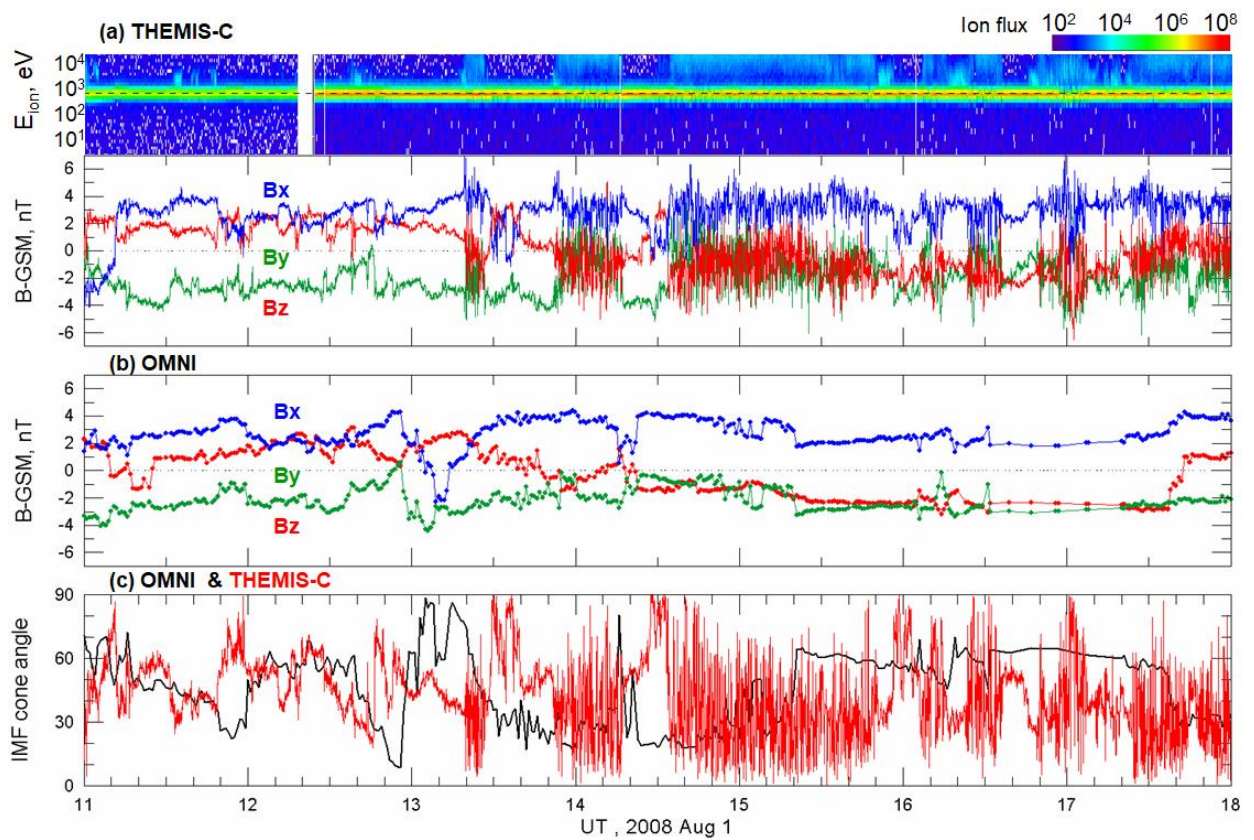


Figure 5. Observations of plasma and magnetic field on August 1, 2008. (a) Ion spectrogram (ion flux is in units of eV/cm² s sr eV) and IMF vector components in GSM coordinates measured by TH-C, (b) IMF vector components from OMNI data set, (c) IMF cone angles plotted for TH-C (red) and OMNI (black).

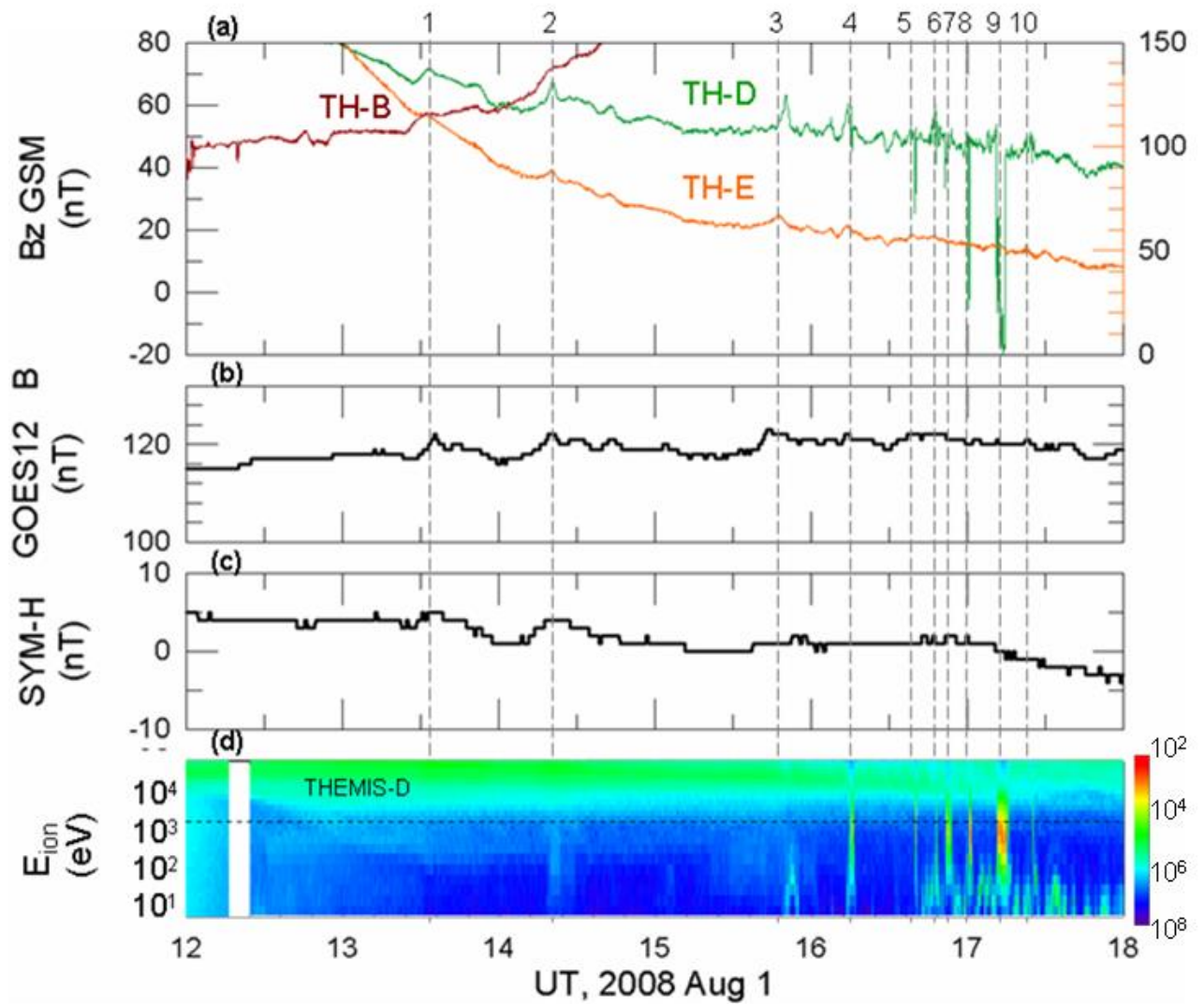


Figure 6. Satellite measurements of magnetic field and plasma in the dayside magnetosphere and geomagnetic activity. (a) The B_z -GSM components from THEMIS probes TH-B (brown), TH-E (orange), and TH-D (green). The left y-axis corresponds to the magnetic measurements from TH-B and TH-D, and the right y-axis to TH-E. (b) The magnetic field strength from GOES-12 (black); (c) the SYM-H index; and (d) the ion spectrogram from TH-D (ion flux is in units of $\text{eV}/\text{cm}^2 \text{ s sr eV}$). Dashed lines, numbered from 1 to 10, indicate time moments of magnetic and plasma disturbances observed by THEMIS.

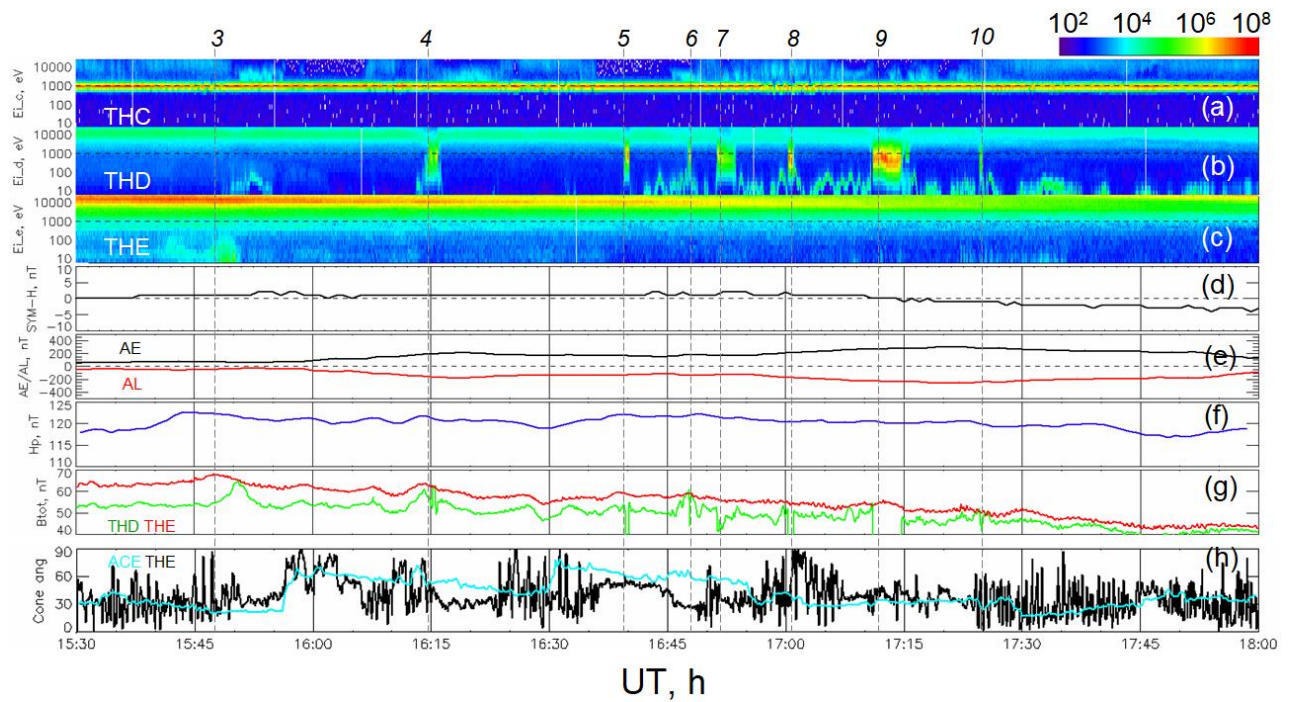


Figure 7. Observations of plasma and magnetic field at 1530-1800 UT on August 1, 2008: (a-c) ion spectrograms measured by TH-C, TH-D, and TH-E (ion flux is in units of $\text{eV}/\text{cm}^2 \text{ s sr eV}$), (d) SYM-H index, (e) AE (black) and AL (red) indices, (f) horizontal magnetic field Hp detected by GOES 12 from 10 to 13 LT, (g) magnetic field strengths Btot from TH-D (green) and TH-E (red), (h) IMF cone angles for TH-C (black) and for the ACE upstream monitor (blue). The ACE measurements are delayed by 60 min. Dashed lines and numbers #4 - #10 mark magnetospheric disturbances with magnetosheath ion population observed in the magnetosphere.

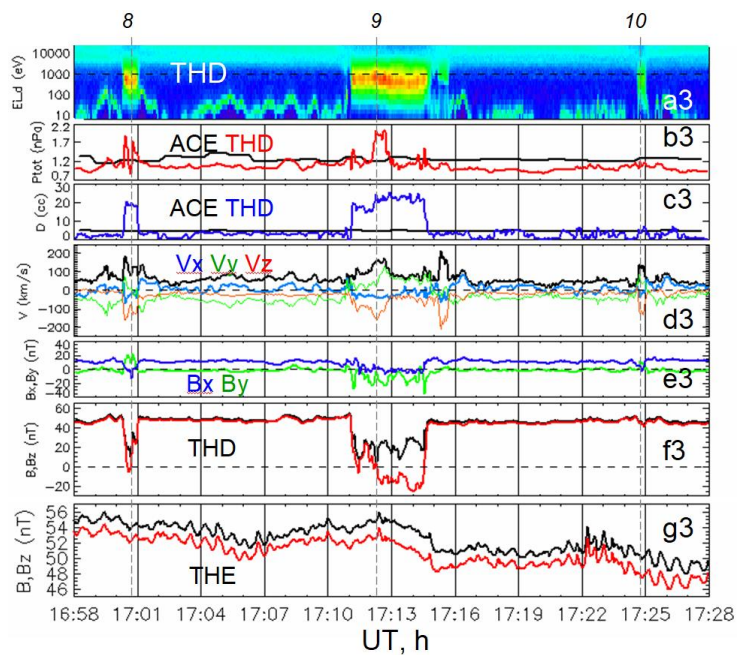
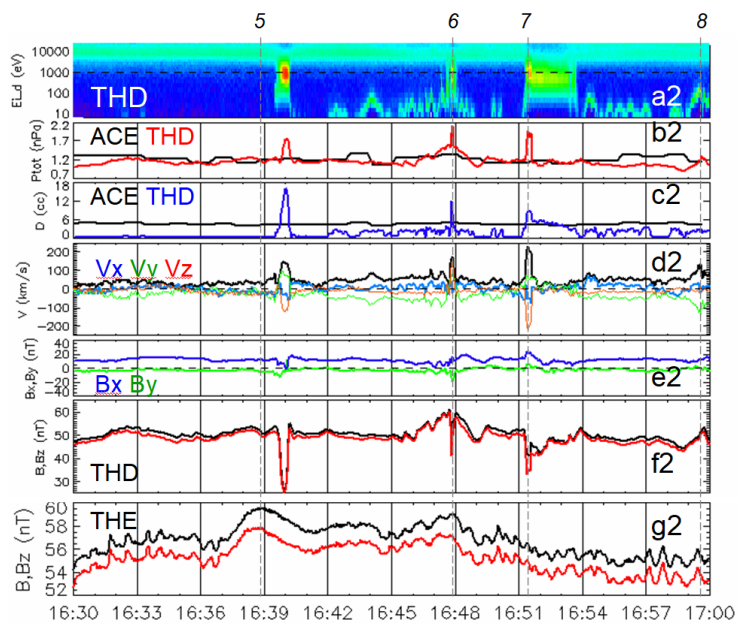
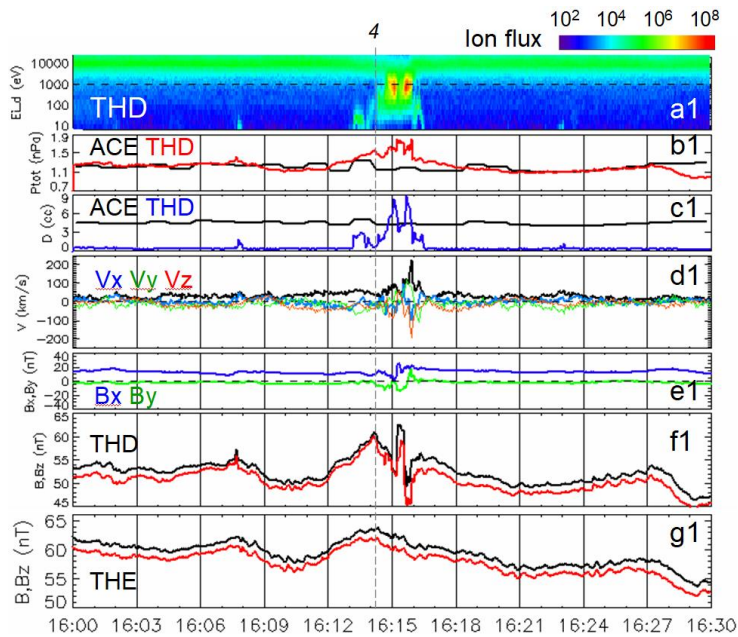


Figure 8. Observations of plasma and magnetic field during the intervals 1600 - 1630 UT, 1630 - 1700 UT and 1658 - 1728 UT on August 1, 2008. Panels show from top to bottom: (a) ion spectrogram from TH-D, (b) total pressure measured by the ACE upstream monitor (black) and TH-D (red), (c) plasma density measured by ACE (black) and TH-D (blue), (d) TH-D measurements of bulk velocity V (black) and its components in GSM coordinates V_x (blue), V_y (green) and V_z (red), (e) transversal components of magnetic field B_x (blue) and B_y (green) from TH-D, (f) magnitude B and B_z component of magnetic field from TH-D, (g) magnitude B and B_z component of magnetic field from TH-E. The magnetosheath plasma penetration is denoted by dashed lines and numbers #4 - #10.

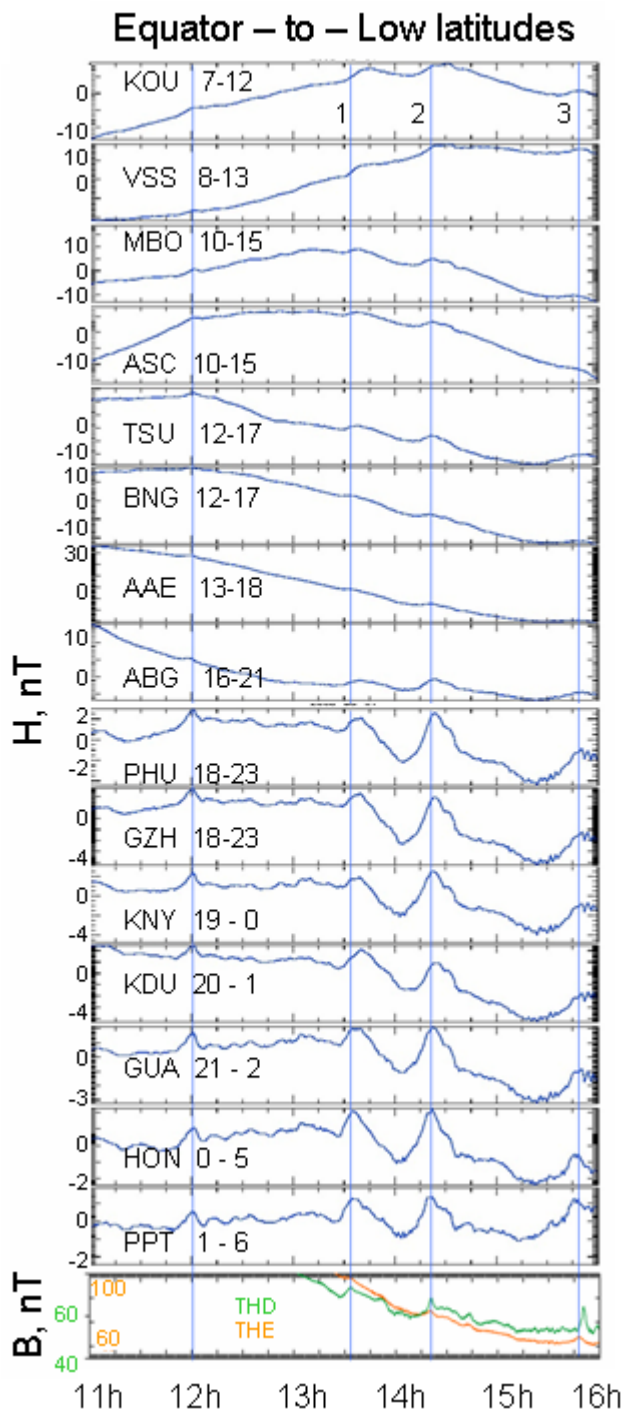


Figure 9. Relative variations in the horizontal component (H) of the geomagnetic field at low geomagnetic latitudes. Local time intervals are indicated near the station codes. The vertical lines depict time of the magnetic pulses at THEMIS (lines #1 - #3). Bottom panel shows magnetic field B measured by TH-E (orange) and by TH-D (green).

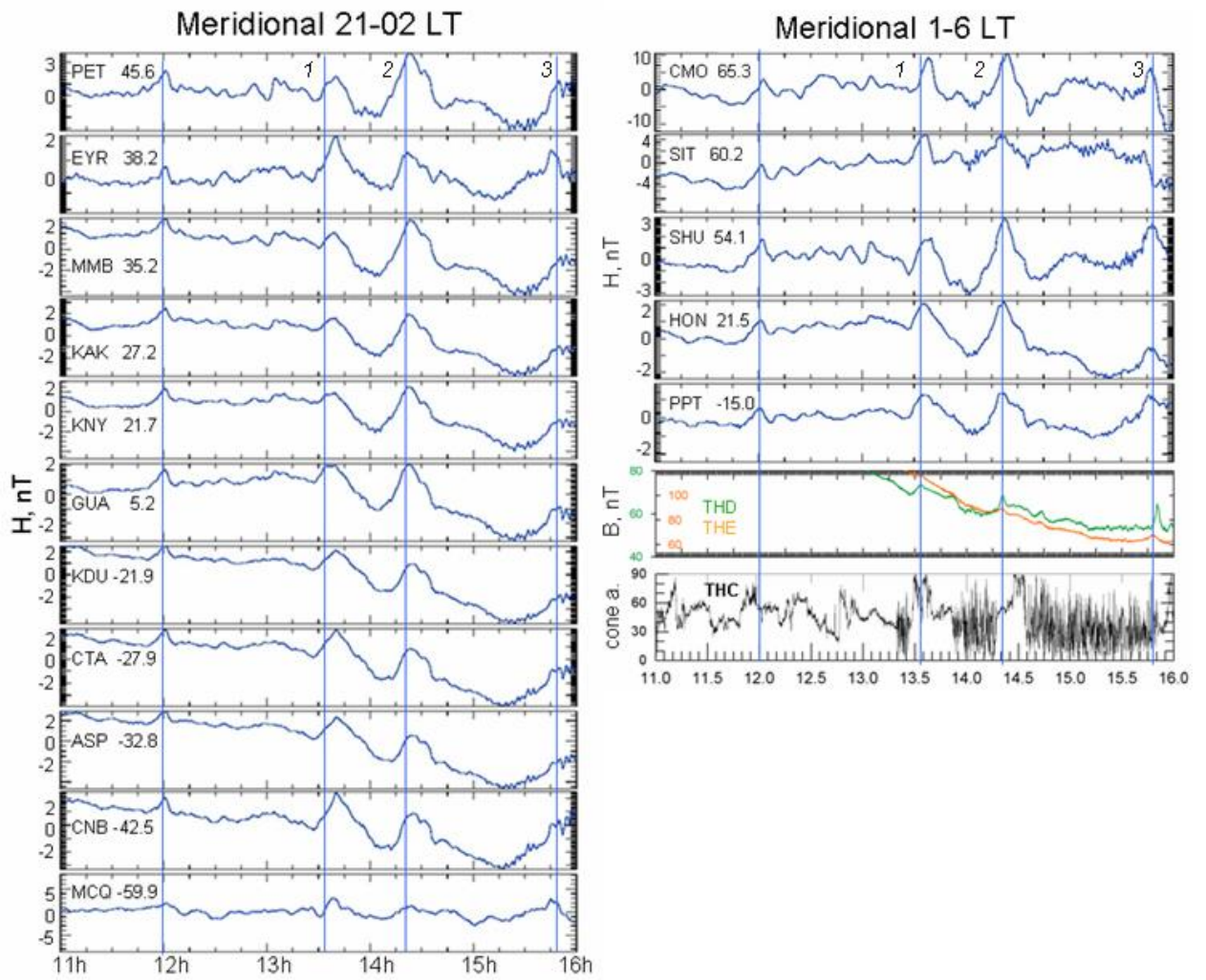


Figure 10. Relative variations in the horizontal component (H) of the geomagnetic field in the midnight (left) and predawn (right) sectors. The geomagnetic latitudes of the stations are indicated near station codes. The vertical lines depict time of the magnetic pulses at THEMIS.

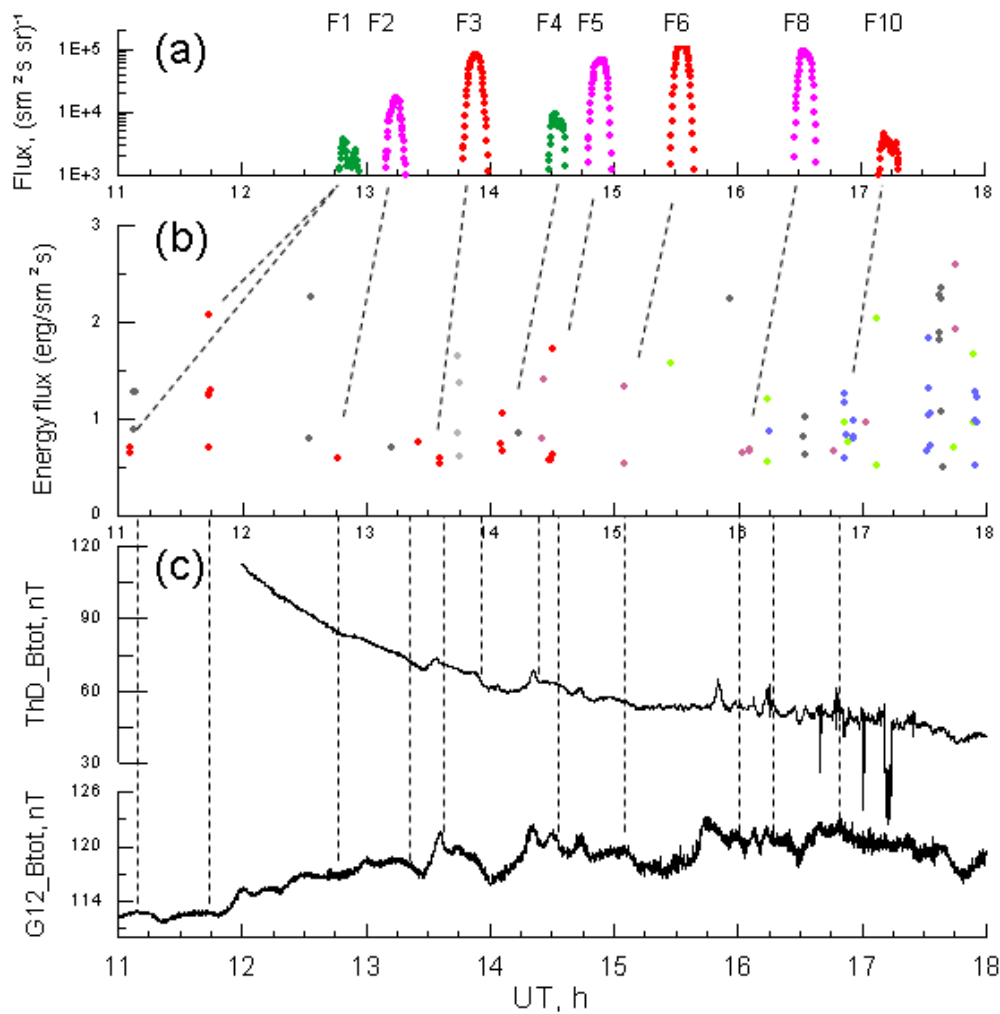


Figure 11. Dynamics of the geomagnetic field and particles on 1 August 2008: (a) FEE enhancements, (b) plasma precipitation at high latitudes, and dayside magnetic field perturbations observed by (c) GOES-12 and (d) THEMIS-D. The numbers indicate the FEE injections at ~ 2 and ~ 5 LT (see Table 1), colors for POES satellite are the same as in Figure 2. Plasma precipitations are shown for the energy flux above the threshold of $0.5 \text{ (erg}/\text{sm}^2 \text{ s)}$ and are grouped in LT: 23 – 24 LT (light gray), 0 – 2 LT (gray), 5 – 6 LT (blue), 12.5 - 15 LT (red points), 15 – 16 LT (violet), and 19.5 – 21.5 LT (green).

Dear Referee1,

Thank you very much for your comments and suggestions. We revised the Discussion and provided additional solid arguments and some quantitative estimation to support our suggestions. Here we try to address all your concerns.

General comments by Referee1:

“This manuscript reports a series of >30 keV electron flux enhancement events that happened at $L < 1.2$ observed by POES satellites, and massive related observations from THEMIS, ground magnetometer, ACE, etc. These events are likely to be a subset of the events analyzed in Suvorova (2017) and this study is a follow-up work related to Suvorova (2017). In the present study, the authors propose that the magnetic perturbation near the magnetopause causes a mixture of magnetosheath plasma and magnetospheric plasma to precipitate in high latitude (high L regions) which further induce a large transient electric field that could transport the electrons to $L < 1.2$. However, there is no solid evidence reported to prove that the flux enhancements at $L < 1.2$ are caused by magnetic perturbation near the magnetopause, nor analysis on the possibilities that this proposed chain of processes could work. The reviewer suggests to at least add in some more solid arguments or simulation results to prove that the proposed processes are reasonable before the paper can be published. The reviewer also suggests the authors to be more concise on some part of the paper, to avoid extra confusions of the readers.”

Reply:

We thank the reviewer for the suggestion which help to improve the manuscript. We provide some additional observations and estimations in Discussion. We revised some descriptions in the paper in order to make them shorter.

In our study, we did not state or suggest that the magnetic perturbations cause the electron enhancements at low L-shells and plasma precipitations at high L-shells. Addressing to the comment 2, we will clarify this crucial point, which is important for overall understanding of our concept.

Specific Comment 1

(1.1) The authors presented the >30 keV electron flux measurements by POES satellites in Figure 1. In Figure 1, it is clear that electron fluxes are enhanced in the quasitrapped region (outside of SAA), but the fluxes in SAA that are more stably-trapped almost remain the same.

Reply:

Actually, electron fluxes did increase in the SAA region. However, the background fluxes in SAA were already high (several units of 10^5 ($\text{cm}^2 \text{ s sr}^{-1}$)). The fluxes of FEE were mostly less than 10^5 ($\text{cm}^2 \text{ s sr}^{-1}$). Hence, they produce a little increase of the flux in SAA which is hard to be seen in the logarithmic scale. However, this effect is beyond the scope of our study.

(1.2) The authors refer to those events as injections in many places in the paper (e.g., line 202, 208). However, if those electrons are injected from higher L, they are supposed to become more 90 degree peaked in pitch angle, which means they are more likely to be stably-trapped and more enhancements in the SAA region are expected. From Figure 1, the slot region is not filled, which is supposed to be seen in a typical injection event that penetrates down to L=1.2. In fact, previous studies such as Li et al (2017, titled "Measurement of electrons from albedo neutron decay and neutron density in near-Earth space") reported events that enhanced stably trapped electrons are observed due to geomagnetic activities while the quasi-trapped electron fluxes stay the same. Moreover, people would easily link the enhancements in the quasi-trapped electrons to enhanced pitch angle scattering. The authors should show more detailed observations of these events and explain why these events are injections.

Reply:

We thank the reviewer for the comment. In order to clarify this crucial issue we revised Figure 2 (see below) in order to show the time profiles of intensities and L-shells of FEE enhancements. As we wrote, we use measurements from the vertically oriented detector ("0-detector") of electrons with local pitch angles of 90° at the equator (quasi or locally trapped electrons). Another detector measured precipitating electrons at the equator. The electron precipitations did not arise. The observed time profiles of quasi-trapped electrons are proper for injections.

We revised the text accordingly:

"Figure 2 and Table 1 present main characteristics of 15 FEE enhancements detected along equatorial passes of POES satellites (P2, P5, P6, P7, P8). We analyze the peak fluxes in the FEE enhancements (time, local time, longitude, and L-shell)."

"As seen in Figure 2a,b, the FEE enhancements peak at minimal L-shells, i.e. at the equator. The fluxes decrease quickly with growing L. This pattern corresponds to a fast radial transport (injection) of electrons from the inner radiation belt. Note that pitch-angular scattering of electrons gives different profiles: the fluxes should be minimal at the equator and grow with L-shell."

Concerning to the albedo neutron mechanism. First of all, that paper is about relativistic electrons (~500 keV) during a geomagnetic storm. We think it has a little relation to our study of low-energy (>30 keV) electrons during nonstorm conditions. Next, it is impossible to apply this mechanism to the FEE enhancements because of the following well known facts: (1) The fluxes of albedo neutrons at equatorial latitudes are much lower (order of magnitudes) than the fluxes of FEE. (2) During magnetic quiet, the latitudinal profile of secondary particles (generated in decay) is positive, i.e. the flux of secondary particles increases with latitude due to a decrease of the cut-off rigidity of incident cosmic rays. Figure 2 demonstrates totally different pattern.

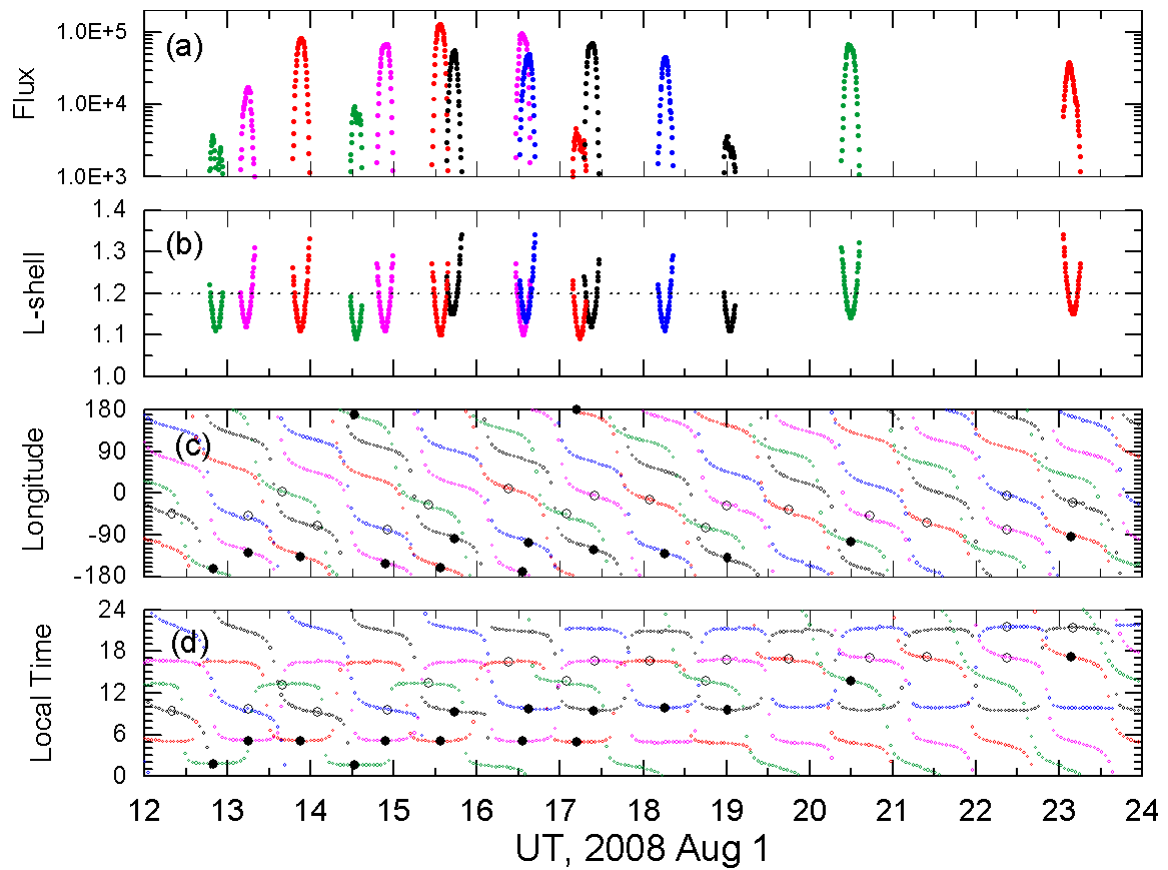


Figure 2 (revised). FEE enhancements on 1 August 2008: (a) fluxes of >30 keV electrons in units $(\text{cm}^2 \text{ s sr})^{-1}$, (b) L-shell of enhancements, (c) longitude and (d) local time of peak fluxes (black circles). Measurements within the SAA area are indicated by the open circles. Colorful curves denote NOAA/POES satellites: P2 (black), P5 (pink), P6 (red), P7 (blue), and P8 (green). Horizontal dashed line at panel (b) depicts the lower edge of the inner radiation belt. FEE enhancements peak at the equator (minimal L-shells) that indicates a fast radial transport from the inner radiation belt.

(1.3) The author should also specify the looking direction of the detector in the caption of Figure 1.

Reply:

In the caption of Figure 1 we add the following sentences:

“The electrons are detected in vertical direction. In the forbidden zone, those electrons are quasi-trapped.”

Specific Comment 2

(2.1) As is stated in the general comments, the authors have not present any solid evidence that the electron enhancements at $L=1.2$ could be caused by magnetic perturbations near the magnetopause which is at quite large L . Only coincidences in time are shown in the present study. The reviewer suggests to show more solid arguments or some simulation results to prove this possibility.

Reply:

We thank the reviewer for the comment, which help to improve the manuscript.

We want to clarify that we did not state that the observed magnetic perturbations near the magnetopause or inside the outer magnetosphere, at large L, can cause such a mixture of plasma at high latitudes and electron enhancements at the equator. These perturbations had small amplitudes of about of several to tens of nT [e.g., line 332]. We wrote [line 513] “A series of night injections of >30 keV electrons could be associated with transient magnetospheric magnetic field perturbations.” We wrote about the association in other parts of text also. Note that the association is not a causality.

In Discussion we add:

“The amplitude of geomagnetic pulses is not very high: from few nT at ground to a few tens of nT at THEMIS. It should be noted that such magnetic perturbations are too weak to produce deep injections of >30 keV electrons below the radiation belt.”

These magnetic perturbations are only a response of the geomagnetic field on occasional pressure pulses produced by magnetosheath plasma jets at the magnetopause. In the study, we emphasized an important role of transient subsolar foreshock condition, under which plasma jets are generated, for the magnetosphere–ionosphere coupling, particularly for non-storm events. The transient subsolar foreshock was only recently recognized as a major driver for a throat aurora at high latitudes, as we mentioned in the study.

In revised Discussion, we emphasize the importance of jets for the magnetosphere-ionosphere coupling under conditions of stable solar wind dynamic pressure and northward IMF:

“The interaction of jets with the magnetopause results in geomagnetic pulses and penetration of the magnetosheath plasma inside the magnetosphere (Figure 8). Note that the upstream conditions observed by THEMIS-C during both time intervals (from 12 to 16 UT and from 16 to 18 UT) were similar in that the quasi-radial IMF appeared. Hence, it is reasonable to suggest that the geomagnetic pulses occurred from 12 to 16 UT were also produced by jets because there were no strong enhancements in the solar wind dynamic pressure P_d . Indeed, as one can see in Figure 1 and 8, gradual tenuous variations of P_d do not exceed a few tenths of nPa and, thus, they cannot produce sharp geomagnetic pulses with amplitudes of ~10 nT.

Also, in the revised manuscript, we provide additional arguments in favor to jet impact on the magnetosphere-ionosphere system. It was established that the impact results in magnetosheath particles precipitations at high latitudes near local noon. We present observations of hot plasma precipitations to the latitude ionosphere during the event:

“The energy fluxes of hot plasma (from 50 eV to 10 keV) are measured by POES/TED plasma spectrometer. We conducted an additional analysis of hot plasma precipitations in the auroral region at L-shells from 7 to ~15 during time interval from 11 to 18 UT on 1 August 2008. Figure 11 demonstrates magnetic observations by THEMIS-D and GOES-12, the energy fluxes of auroral precipitations, and FEE injections. We consider intense precipitations with the threshold of $0.5 \text{ (erg cm}^{-2} \text{ s}^{-1}\text{)}$, which is several times higher than the background. One can see that from 11

to 16 UT, the hot plasma precipitates mainly on the dayside (12 – 16 LT) while after 16 UT, the precipitations occur practically at all local times both on the day and night sides.

The first FEE injection (F1) at ~1250 UT was preceded by several geomagnetic pulses observed by GOES-12 from 1100 to 1230 UT. The pulses were not very prominent because, at that time, GOES-12 was located in the morning sector. One can see that some of pulses were accompanied by dayside auroral precipitations of the hot plasma. Note that POES satellites have 100 min orbital period and, hence, they can miss some of localized precipitations. On the other hand, when a jet hits the magnetopause, the magnetosheath plasma is not necessarily penetrating into the dayside magnetosphere and, hence, precipitating at high latitudes [Dmitriev and Suvorova, 2015]. Nevertheless, in Figure 11, we find two cases of geomagnetic pulses followed by intense dayside precipitations of the hot plasma at 1105 UT and 1144 UT.

Energetic electrons take a certain time dT to drift from the inner radiation belt edge (at L-shell $L_1 = 1.2$) to the heights of ~900 km (L-shell $L_2 = 1.1\sim 1.15$):

$$dT(s) = 6380 * (L_1 - L_2) / V_{DE} \quad (1)$$

where the ExB drift velocity is determined as

$$V_{DE} = 0.032 * L^3 * E, \quad (2)$$

where L the average L-shell in the first approach and E is azimuthal electric field in mV/m. From equations (1) and (2), we estimate that the earthward drift of energetic electron across the magnetic field lines from $L = 1.2$ to $L = 1.1$ takes up to 40 min under local electric field of ~5 mV/m. Note that $E \sim 5$ mV/m was obtained in simulations of energetic electron injections at $L < 1.3$ [Selesnick et al., 2016].

In our case of non-storm conditions, it is hard to imagine that the strong azimuthal E can persist for so long time. Previously, simulations by Su et al. (2016) have showed that it is not necessary for electrons to be transported earthward all the way during a single injection. Hence, we can consider a multi-step radial transport produced by a number of short pulses of E . In this case, the drift from $L=1.2$ to $L=1.1$ requires two or more pulses of ~10 min duration that is comparable with the duration of jet-related disturbances. The multi-step process is limited by the time, during which a particle stays in the region of injection. The >30 keV electrons have a long period of azimuthal drift and, thus, they can stay in the region for hours. In contrast, the >100 keV electrons with the azimuthal period of ~6 h leave quickly the injection region and, thus, do not have enough time to penetrate to the forbidden zone. This effect can explain the absence of high-energy electrons in the FEE enhancements presented.

We can suggest that the first FEE injection required a long time (~hour and longer) and several pulses of E in order to transport energetic electrons from undisturbed edge of the inner radiation belt to $L\sim 1.1$. Then, >30 keV electrons populate L-shells from 1.15 to 1.1 that makes possible to transport electrons to 900 km heights for a short time of ~10 min by one pulse of strong E . The latter pattern is applicable for the FEE injection F2 and subsequent others. As one can see in Figure 11, each FEE injection after 13 UT is preceded within <30 min by intense auroral precipitations of the hot plasma. The latter is accompanied with geomagnetic pulses produced by the interaction of jets with the magnetopause. It is important to remind that tenuous variations of the solar wind dynamic pressure could not produce the geomagnetic perturbations occurred during the interval considered.

We associate the dayside precipitations at high latitudes with the effect of jets piercing the magnetopause. The jets provide penetration of hot plasma from the magnetosheath to the magnetosphere. Dmitriev and Suvorova (2015) have found that the average rate of jet-related penetration of the magnetosheath plasma into the magnetosphere is about 10^{29} particles per day.

The penetrated hot ions move quickly (within a few minutes) along the magnetic field lines to high-latitude regions of the dayside ionosphere. We can estimate the flux of precipitating ions of $\sim 10^7$ to 10^8 ($\text{cm}^2 \text{s}^{-1}$) if we assume that particles precipitate on the dayside arc of 3° width at 70° latitude. This particle flux corresponds well to the energy fluxes of precipitating ions ($>0.5 \text{ erg cm}^{-2} \text{ s}^{-1}$) measured by POES/TED at high latitudes (see Figure 11). Hence, the jet-related magnetosheath plasma can produce significant additional ionization and increase conductivity of the high-latitude ionosphere on the dayside. An enhancement of electric currents in the dayside ionosphere should induce an enhancement of the electric field on the nightside and especially in the predawn sector, where the conductivity is weak. The nightside electric field might penetrate from high to low latitudes and produce ExB drift of electrons from the inner radiation belt to lower heights.”

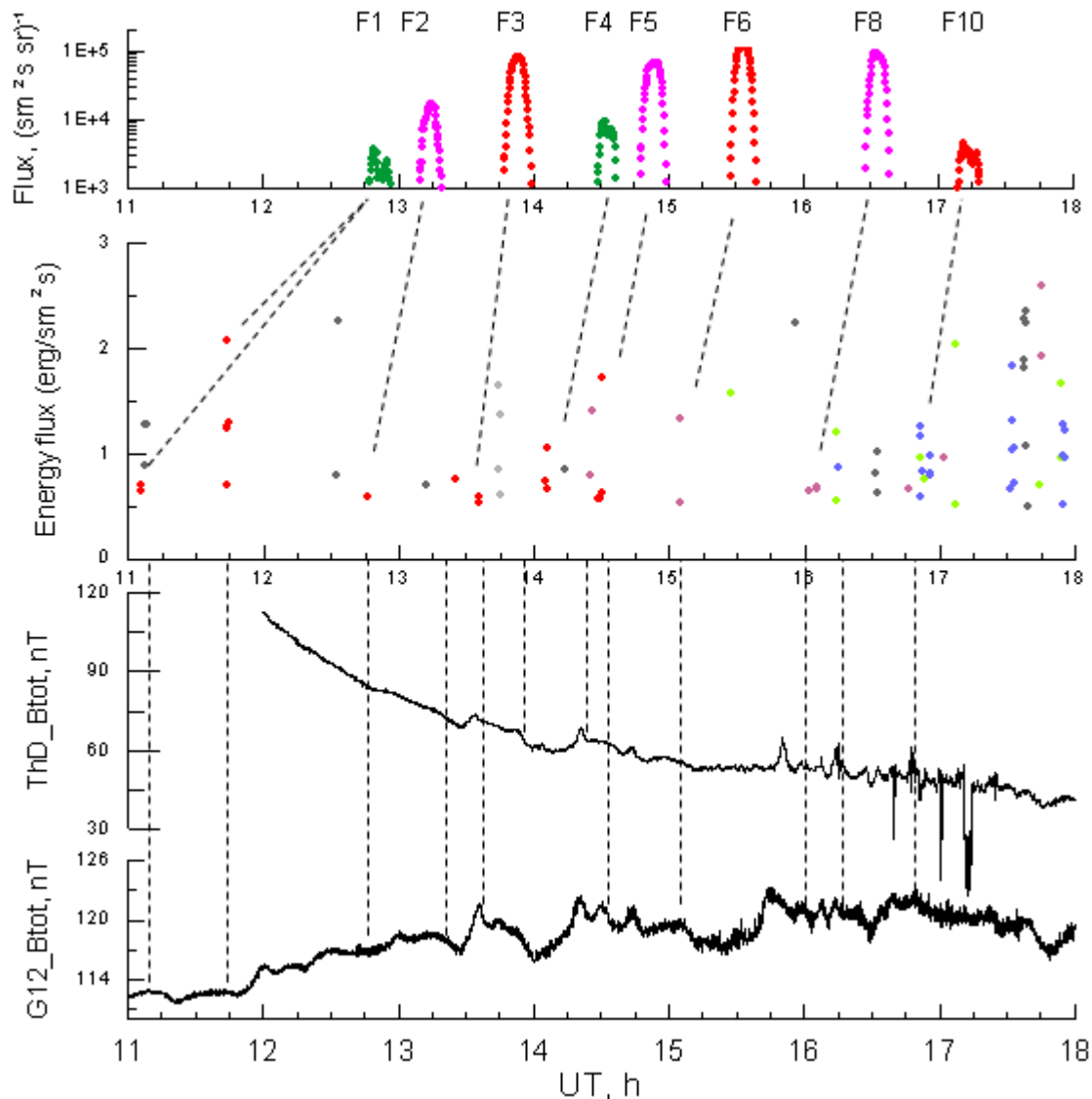


Figure 11.

(2.2) In Li et al (2017), which is mentioned above, they also state that the large electric field can only cause an L shell distortion of 0.01 and this process is energy-dependent. Please comment on it and the possibility that the electric field moves the electrons to $L < 1.2$ in this case.

Reply:

We note that Li et al. indicated the L-shell distortion of 0.01 for the relativistic electrons but not for the low-energy of 30 keV. In this concern, they cited the studies by Selesnik et al (2016) and Su et al. (2016), where observations of electron injections below $L = 2$ were compared with simulations. According to Su et al., “the electric field does not have a significant impact for electrons with energy >400 keV in the inner belt” (on page 8520), and “an enhanced large-scale electric field can be responsible for injection of ~ 100 keV electrons in the inner radiation belt” (on page 8521).

Also, it is important that they emphasized that “it is thus not necessary for electrons to be transported all the way from the outer zone during a single injection.” Hence, as followed from this, the slot region is not necessary to be filled by enhancements (see Referee’s comment 1).

Selesnik et al. investigated various models of electric fields in applicability for deeper injections at $L < 1.2$. Their conclusion is “Injection to $L < 1.2$ is demonstrated in both observations and simulations by the end of 23 June, but the simulated injection is smaller because the model E_c (electric field) was reduced to zero for $L < 1.17$ ”.

The simulations showed that at $L < 1.3$ during quiet condition, an average electric field is weak (~ 0.4 mV/m), but for deep injections the field should be strong ~ 5 mV/m. Hence, the simulation studies had to admit that strong electric fields could penetrate and cause deep injections at $L < 1.3$, but mystery of a penetration mechanism was not disclosed.

We put attention that, in our “quiet” case the penetration electric field could not be generated in a storm/substorm process. What process could provoke such a strong electric field at $L < 1.3$?

The both studies pointed out that none of the existing models can accurately describe the penetration electric field and, hence, deep injections at $L < 1.2$. Su et al. (2016) : “An accurate global electric field model is a necessary requirement in order to correctly capture the non-diffusive radial transport in the inner radiation belt.” Our paper presents new experimental results, which help to develop a new model. The new model should be a subject of another study.

Specific Comment 3

(3) In Table 1, the authors list a series of flux enhancement events observed by POES. The author should specify the criteria used to select those events, and show some detailed electron flux profile of those events, such as how long the enhancements last, specific L shell of each event or how many data points are included in each event. The reviewer also suggests to use more commonly used names for POES satellites such as POES-15/18...instead of P2/P5...

Reply:

In the revised Figure 2, the intensity and L-shells of enhancements are shown. In the revised manuscript, we specify the criteria more precisely:

“... the forbidden zone extends at $L < 1.2$ in the latitudinal range from -20° to $+30^\circ$ and in the longitudinal range from 0° to 260°E (or 100°W) that is beyond the South Atlantic anomaly (SAA). ... Figure 1b shows the interval 12 - 24 UT, when fluxes of >30 keV quasi-trapped electrons in the forbidden zone increased by 3 orders of magnitude above a background of $\sim 10^2$ ($\text{cm}^2 \text{ s sr}^{-1}$) and kept at the enhanced level for several hours. **We have selected FEE enhancements with intensity $>10^3$ ($\text{cm}^2 \text{ s sr}^{-1}$).**”

We think that abbreviation P2, P5 etc. are more convenient for presentations in Figures and Tables. Moreover, we would keep the abbreviations, which we used in our previous papers.

Specific Comment 4

(4) Line 210-227: the authors intend to prove that each flux enhancement event is individual and not caused by any other event, for example, F2 is not caused by F1. However, this analysis is based on the presumption that the event is really transient. The authors should show some evidence to argue such as F1 could not have been enhanced 100 min before the observation of F1. Also, please explain why this is important. The reviewer does not find it very essential to the analysis later and suggests to be more concise on this problem.

Reply:

In the original manuscript, we have already clarified this important issue: “Figure 1a shows the observations of the >30 keV electrons at 0 - 12 UT, before the enhancements occurred.”

In the revised manuscript we provide an additional explanation:

“At that time, the satellites passed the same regions but they did not detect any FEE enhancements.”

The suggestion of multiple injections is important because several injections are accompanied by several jets. We find correspondence between the jets/pressure pulses and injections (Figure 11).

Note that there were no substorm-associated injections in the present case.

Specific Comment 5

(5) Line 227: Please specify if these events are a subset of Suvorova (2017) event list. If so, the authors should make a clarification before stating that the characteristics agree with those in Suvorova (2017), otherwise it is misleading.

Reply:

This event (15 peaks in one day) is a subset (1%) of the total statistics of 2465 peaks at the equator within 530 days. Examples of storm and nonstorm enhancement events (including the interval of 1 - 3 August 2008) were presented in Figure 1 of the paper by Suvorova (2017). We mention it in Introduction of the revised manuscript:

“Note that this event is a subset (1%) of the total statistics collected by Suvorova (2017) during various conditions, from magnetic quite to extremely strong geomagnetic storms.”

Generally speaking, an individual event could be different from the overall statistics regarding the location of injections (local time and longitude ranges), especially for such specific conditions. Indeed, this particular event occurred under very quiet geomagnetic condition, while the vast majority of events with similar parameters, such as multiple peaks or long durations of

>4 h and high peak intensity $> 10^4 - 10^5 \text{ (cm}^2 \text{ s sr)}^{-1}$ occurred mainly during storms/substorms. Nevertheless, the electron enhancements during the August 1, 2008 event are in well agreement with those found from statistics as we concluded in the original manuscript (lines 223 – 227): namely:

“specific longitudinal and local time distributions of the enhancements indicate multiple injections during about 4.5 h in the sector of 0 - 6 LT, and the injection region was confined within 3 h of local time over central and eastern Pacific. In general, these characteristic of injections are in well agreement with those found from statistics (Suvorova, 2017).”

Specific Comment 6

(6) Figure 3: Since the authors show that L1 is not a preferable location for observations of the magnetic perturbations as compared to Themis, this figure is not necessary. The reviewer suggests to combine some of the information in Figure 3 into Figure 4 and be more concise on the text as well, in order to help the readers to focus on the important part, Themis observations.

Reply:

The Figure 3 is important at least because of the comment by Referee 2, who believes that variation in the solar wind dynamic pressure could cause these magnetospheric compressions. The Figure clearly demonstrates that variations are tenuous. Additionally, a discussion of the OMNI data is important due to its wide use.

Specific Comment 7

(7) Line 611: Please use explicit number of the latitude of throat aurora instead of “lower latitude” here. It is misleading because this study is talking about phenomena at $L=1.2$ (<30 deg in latitude), while the throat aurora in a series of Han et al papers is still located at >70 deg in latitude (or please correct this number).

Reply:

Thank you for the important comment. We revised the text accordingly:

“Sometimes, the dayside aurora penetrates to lower [geomagnetic latitudes of \$\sim 72^\circ\$ from the discrete aurora oval at geomagnetic latitude \$\sim 76^\circ\$](#) , so-called throat aurora.”

Sincerely,
Alla Suvorova

Dear Referee2,

Thank you very much for your comments and suggestions. We revised the Discussion and provided additional solid arguments and some quantitative estimations to support our suggestions.

General Comments by Referee2:

This paper reports energetic (>30 keV) electron flux enhancement at $L<1.2$ measured by the NOAA/POES satellites and relate it to the transient injection of magnetosheath plasma into the dayside magnetopause region, which is measured by the THEMIS satellite, and global geomagnetic pulses, which are measured by ground INTERMAGNET magnetometers and GOES satellites. The authors propose a scenario of possible association between these dayside magnetopause phenomena with the deep injection of >30 keV electrons at $L<1.2$ by the penetration of localized electric field.

The electron flux enhancement at $L<1.2$ is well described including its research history which is very interesting. Looking through this paper, however, I think the connection between the observed phenomena occurring in the dayside magnetosheath/magnetopause region and the electron flux enhancement at $L<1.2$ is weak and not well validated by the observations reported in this paper. These two phenomena occur in the same half day of 12-24 UT on August 1, 2008. But there is a significant possibility that they occur in the same day “by chance”. I think it is necessary to provide some more concrete evidence including some quantitative estimation that can explain the observed $L<1.2$ electron enhancement.

Reply:

We thank the reviewer for the suggestion which help to improve the manuscript. In the revised manuscript, we add some estimation on ExB drift. We provide additional arguments in favor to jet impact on the magnetosphere-ionosphere system. We present observations of hot plasma precipitations to the high-latitude ionosphere during the event in a new Figure 11. It was established that the jet impact results in magnetosheath particles precipitations at high latitudes near local noon. In Discussion we add:

“The energy fluxes of hot plasma (from 50 eV to 10 keV) are measured by POES/TED plasma spectrometer. We conducted an additional analysis of hot plasma precipitations in the auroral region at L -shells from 7 to ~ 15 during time interval from 11 to 18 UT on 1 August 2008. Figure 11 demonstrates magnetic observations by THEMIS-D and GOES-12, the energy fluxes of auroral precipitations, and FEE injections. We consider intense precipitations with the threshold of 0.5 ($\text{erg cm}^{-2} \text{s}^{-1}$), which is several times higher than the background. One can see that from 11 to 16 UT, the hot plasma precipitates mainly on the dayside (12 – 16 LT) while after 16 UT, the precipitations occur practically at all local times both on the day and night sides.

The first FEE injection (F1) at ~ 1250 UT was preceded by several geomagnetic pulses observed by GOES-12 from 1100 to 1230 UT. The pulses were not very prominent because, at that time, GOES-12 was located in the morning sector. One can see that some of pulses were accompanied by dayside auroral precipitations of the hot plasma. Note that POES satellites have 100 min orbital period and, hence, they can miss some of localized precipitations. On the other hand, when a jet hits the magnetopause, the magnetosheath plasma is not necessarily penetrating into

the dayside magnetosphere and, hence, precipitating at high latitudes [Dmitriev and Suvorova, 2015]. Nevertheless, in Figure 11, we find two cases of geomagnetic pulses followed by intense dayside precipitations of the hot plasma at 1105 UT and 1144 UT.

Energetic electrons take a certain time dT to drift from the inner radiation belt edge (at L-shell $L_1 = 1.2$) to the heights of ~ 900 km (L-shell $L_2 = 1.1\sim 1.15$):

$$dT(s) = 6380 * (L_1 - L_2) / V_{DE} \quad (1)$$

where the ExB drift velocity is determined as

$$V_{DE} = 0.032 * L^3 * E, \quad (2)$$

where L the average L-shell in the first approach and E is azimuthal electric field in mV/m. From equations (1) and (2), we estimate that the earthward drift of energetic electron across the magnetic field lines from $L = 1.2$ to $L = 1.1$ takes up to 40 min under local electric field of ~ 5 mV/m. Note that $E \sim 5$ mV/m was obtained in simulations of energetic electron injections at $L < 1.3$ [Selesnick et al., 2016].

In our case of non-storm conditions, it is hard to imagine that the strong azimuthal E can persist for so long time. Previously, simulations by Su et al. (2016) have showed that it is not necessary for electrons to be transported earthward all the way during a single injection. Hence, we can consider a multi-step radial transport produced by a number of short pulses of E . In this case, the drift from $L=1.2$ to $L=1.1$ requires two or more pulses of ~ 10 min duration that is comparable with the duration of jet-related disturbances. The multi-step process is limited by the time, during which a particle stays in the region of injection. The >30 keV electrons have a long period of azimuthal drift and, thus, they can stay in the region for hours. In contrast, the >100 keV electrons with the azimuthal period of ~ 6 h leave quickly the injection region and, thus, do not have enough time to penetrate to the forbidden zone. This effect can explain the absence of high-energy electrons in the FEE enhancements presented.

We can suggest that the first FEE injection required a long time (\sim hour and longer) and several pulses of E in order to transport energetic electrons from undisturbed edge of the inner radiation belt to $L\sim 1.1$. Then, >30 keV electrons populate L-shells from 1.15 to 1.1 that makes possible to transport electrons to 900 km heights for a short time of ~ 10 min by one pulse of strong E . The latter pattern is applicable for the FEE injection F2 and subsequent others. As one can see in Figure 11, each FEE injection after 13 UT is preceded within <30 min by intense auroral precipitations of the hot plasma. The latter is accompanied with geomagnetic pulses produced by the interaction of jets with the magnetopause. It is important to remind that tenuous variations of the solar wind dynamic pressure could not produce the geomagnetic perturbations occurred during the interval considered.

We associate the dayside precipitations at high latitudes with the effect of jets piercing the magnetopause. The jets provide penetration of hot plasma from the magnetosheath to the magnetosphere. Dmitriev and Suvorova (2015) have found that the average rate of jet-related penetration of the magnetosheath plasma into the magnetosphere is about 10^{29} particles per day. The penetrated hot ions move quickly (within a few minutes) along the magnetic field lines to high-latitude regions of the dayside ionosphere. We can estimate the flux of precipitating ions of $\sim 10^7$ to 10^8 ($\text{cm}^2 \text{s}^{-1}$) if we assume that particles precipitate on the dayside arc of 3° width at 70° latitude. This particle flux corresponds well to the energy fluxes of precipitating ions (>0.5 erg $\text{cm}^{-2} \text{s}^{-1}$) measured by POES/TED at high latitudes (see Figure 11). Hence, the jet-related magnetosheath plasma can produce significant additional ionization and increase conductivity of the high-latitude ionosphere on the dayside. An enhancement of electric currents in the dayside ionosphere should induce an enhancement of the electric field on the nightside and especially in

the predawn sector, where the conductivity is weak. The nightside electric field might penetrate from high to low latitudes and produce ExB drift of electrons from the inner radiation belt to lower heights.”

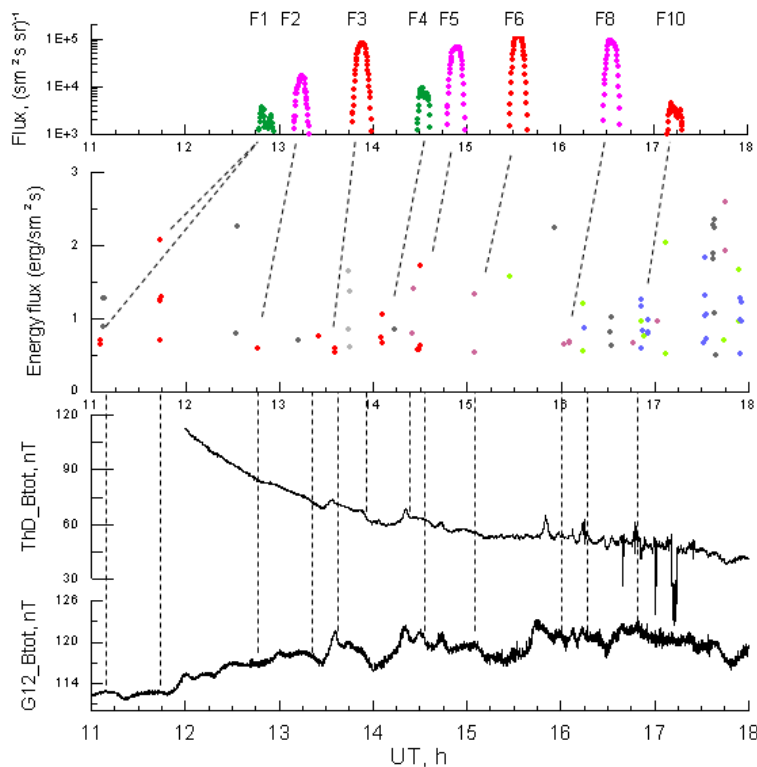


Figure 11. Dynamics of the geomagnetic field and particles on 1 August 2008: (a) FEE enhancements, (b) plasma precipitation at high latitudes, and dayside magnetic field perturbations observed by (c) GOES-12 and (d) THEMIS-D. The numbers indicate the FEE injections at ~2 and ~5 LT (see Table 1), colors for POES satellite are the same as in Figure 2. Plasma precipitations are shown for the energy flux above the threshold of 0.5 (erg/sm² s) and are grouped in LT: 23 – 24 LT (light gray), 0 – 2 LT (gray), 5 – 6 LT (blue), 12.5 - 15 LT (red points), 15 – 16 LT (violet), and 19.5 – 21.5 LT (green).

Specific Comment 1

1. The descriptions of OMTI, THEMIS, GOES and ground magnetometers are fair and easy to understand, although they can be shorter. The authors propose a scenario that dayside magnetopause phenomena cause magnetosphere compression, and associated magnetosheath / magnetospheric plasma precipitation to the dayside ionosphere at high latitudes that result in a local increase of the ionospheric conductivity. This in turn promotes generation of transient localized electric fields, which are able to penetrate from high latitudes to very low latitudes to accelerate energetic electrons at $L < 1.2$. However, in the nightside auroral zone we have normal aurora and associated ionospheric conductivity change which can be much larger than those in the dayside aurora. If the scenario proposed by the authors works, why we do not have $L < 1.2$ acceleration during ordinary (non-storm time) substorms which occur almost every day and cause strong aurora and associated conductivity change in the nightside high latitudes? If $L < 1.2$ electron flux enhancement does not occur during ordinary substorms, I think it indicates that the proposed scenario does not work in the actual magnetosphere.

Reply:

Indeed, a typical substorm produces an increase of conductivity on the nightside. In contrast, our scenario is proposed for the magnetic quiet (no substorm!) and it is based on the change of

dayside conductivity, which should be larger than the nightside one. The scenario explains qualitatively the induction of electric field on the nightside.

It is true that not every substorm results in FEE enhancement. It means that substorm activity alone is insufficient for induction and penetration of electric field to low latitudes on the nightside. We also pointed out this important issue in Introduction of original manuscript [lines 137-146]. Namely, the FEE events account for only 8% of the total time from 1998 to 2016 (Suvorova, 2017). Most of FEE events are accompanied by substorm activity, but we have found “three dozen days without essential substorm activity”. Hence, it should be something else. Here, we totally agree with the Reviewer.

It seems the factor controlling the occurrence of FEE enhancements might be different for storm-time and non-storm conditions. In the previous study, we have found that the illumination of the dayside auroral zone plays the key role, because its dependence on tilt angle explains perfectly the annual variation of FEE occurrence with a main maximum during the northern summer period, from May to September (see Figure 13 in Suvorova, 2017). In order to clarify this important issue, we have revised the end of Introduction accordingly:

“External drivers from the solar wind should trigger some processes in the magnetosphere-ionosphere system that might result in the electron injections into the forbidden zone. However, the external drivers are necessary but often not sufficient for FEE enhancements to occur. If the auroral ionosphere is sunlit, then impact of external drivers more likely results in the electron injections into the forbidden zone. In this case, the factor of the dayside auroral ionosphere conductivity is sufficient, and it comes to the fore during weak geomagnetic activity. The relevant processes in the magnetosphere-ionosphere chain during magnetic quiet are still unclear.”

In order to clarify the role of the dayside conductivity in the auroral zone, we add Figure 11 (see above). As known, the initial response to the solar wind impact is particle precipitations to the high-latitude ionosphere at the dayside, particularly within the cusp region. For example, impact of high solar wind pressure under northern IMF Bz. It is a very common case to observe dayside aurora and intense particle precipitations in the cusp. Under non-substorm condition, intense dayside particle precipitations in sunlit auroral zone can provide a temporal condition for a higher conductivity at the dayside. In such condition, the electric field is induced in the nightside ionosphere (where the conductivity is relatively lower) and then the induced electric field might penetrate to low latitudes providing the earthward transport of particles. Hence the additional ionization of sunlit auroral zone is a very important condition in the proposed scenario. We have to remind that the mechanism of the electric field penetration is still unresolved problem of the magnetospheric physics.

Specific Comment 2

2. As shown in Figures 7 and 8 the THEMIS satellites shows repeating motion in and out from the magnetosphere to the magnetosheath. Such in and out features are very often seen when THEMIS is approaching to the magnetopause region, because the magnetopause location is not fixed and changes due to dynamic pressure change in the magnetosheath and/or surface waves caused by Kelvin-Helmholtz instability in the magnetopause. In the present case, since compressional wave signatures are seen in GOES and ground magnetometers, it is likely that the dynamic pressure variation outside the magnetosphere is the cause of this motion of THEMIS in/out from the magnetosphere. But I think such compressional wave with an amplitude of a few nanotesla is not unusual and occur frequently. Then how often does the authors find $L < 1.2$ electron acceleration? Is this a frequent phenomenon occurring associated with the frequently-occurring compression of the magnetosphere with the amplitude of a few nano-tesla on the ground magnetometers? How the authors can prove that these two phenomena occurs in the same time not by chance? Maybe the authors can check correspondence of timing between each magnetospheric compression and the electron flux enhancement at $L < 1.2$.

Reply:

We have partially replied to this comment above (see Reply to General comment). Concerning to the magnetopause motion and magnetic variations in our case, the weak magnetic pulses do not affect the FEE enhancements. They are just signatures of jets impacting the magnetopause. In the scenario proposed, the key effect is the jet-related penetration of the magnetosheath plasma inside the magnetosphere and its precipitation to the dayside auroral ionosphere. Actually, only a small portion of jets (~10%) pierces the magnetopause. In the revised manuscript, we mention:

“On the other hand, when a jet hits the magnetopause, the magnetosheath plasma is not necessarily penetrating into the dayside magnetosphere and, hence, precipitating at high latitudes [Dmitriev and Suvorova, 2015].”

This is why not every magnetic pulse is followed by FEE enhancement. Considering Figure 11 in the revised manuscript, we demonstrate the direct relationship between jets, magnetosheath plasma penetration/precipitation and FEE injections.

Specific Comment 3

3. The authors show magnetic field pulses observed by GOES and ground magnetometers. If the penetrating electric field is propagating in the magnetosphere, it should be related to the observed magnetic field variations by the Maxwell's equation of $dB/dt = -\text{rot } E$. One can argue that the observed magnetic field variation (dB/dt) can be used to estimate electric field by taking only one component of the rotation, e.g., $dB/dt = dE_x/dy$ ($dE_x = dB/dt * dy$). The GOES magnetic field amplitude is ~5 nT and the time scale was ~500 s. If we take a localized scale size of $dy = 1000$ km, it gives the electric field intensity of 0.01 mV/m ($= 1000 \times 10^{-3} \times 5 \times 10^{-9} / 500$). This value seems to be too small to cause the electron flux enhancement at $L < 1.2$, because this value is two orders smaller than the prevailing electric field in the ionosphere by the thermospheric neutral wind through F-region dynamo. Thus, electric field associated with the observed magnetospheric compression seems not to work for the present case.

Reply:

We agree that the magnetic field pulses were too weak to provide the FEE injections. To make the text clear, in Discussion we add:

“The amplitude of geomagnetic pulses is not very high: from few nT at ground to a few tens of nT at THEMIS. It should be noted that such magnetic perturbations are too weak to produce deep injections of >30 keV electrons below the radiation belt.”

Specific Comment 4

4. In Figure 2b, I noticed that not only the electron flux at $L < 1.2$, but also the electron flux at high latitudes above ± 60 degree increases, particularly at negative longitudes in the northern hemisphere and positive longitudes in the southern hemisphere. Thus the electron acceleration seems to be not confined at $L < 1.2$. Why the authors neglect this clear enhancement of electron flux about ± 60 degrees? It is not clear whether the flux at middle latitudes increased or not in this color scale. If possible, it would be better to show the latitudinal profile of electron flux changes at some particular longitudes (e.g., at -120 degree) in a separated figure. Such figure may be useful to discuss how the electric field penetration suggested by the authors affect from high to low latitudes.

Reply:

We thank the Referee for the valuable comment.

Concerning the mechanisms of radial transport, we wrote in Introduction [lines 55-61] that studies (e.g., Turner, 2015) showed that mechanisms of injections and dynamics of energetic electrons at low L-shells (inside the plasmasphere, $L < 4$) are different from those at higher L-shells (outside the plasmasphere). Nevertheless, we have checked > 30 keV electron fluxes at high latitudes using data from both detectors measured precipitating and trapped populations of the outer radiation belt. We found that the fluxes of the radiation belt electrons increased after 16 UT. Note that increases of electron fluxes at high latitudes observed at low-earth's orbits are rather caused by pitch-angular scattering of trapped electrons into the loss cone due to wave activity rather than due to the effect of electric field.

From 12 to 16 UT the electron fluxes at high latitudes were not disturbed in contrast to FEE at low latitudes. Note that at middle latitudes, the satellites measured the background intensity of precipitating electrons from the inner radiation belt, while trapped population was observed in the SAA region ($L < 2$). As seen in Figure 1 (a, b), the background fluxes in SAA were already high (several units of 10^5 ($\text{cm}^2 \text{ s sr}^{-1}$)), and the fluxes of FEE were mostly less than 10^5 ($\text{cm}^2 \text{ s sr}^{-1}$). Hence, they produce a little increase in the flux at $L < 2$.

At higher L-shells, the increase could be even less. Let assume that the induced electric field accelerates electrons in the radiation belt. In this case, the electrons should stay in the acceleration region for a certain time, which should be sufficient for effective acceleration. In Discussion we consider this situation for > 100 keV electrons in the inner radiation belt:

“In contrast, the >100 keV electrons with the azimuthal period of ~ 6 h leave quickly the injection region and, thus, do not have enough time to penetrate to the forbidden zone. This effect can explain the absence of high-energy electrons in the FEE enhancements presented.”

Similarly at high latitudes, i.e. for the outer radiation belt (L-shells ~ 4), we can find that ~ 30 keV electrons have azimuthal period of ~ 6 h and, thus, they leave quickly the acceleration region and gain not too much energy. So the flux increase (if any) is hard to be seen in the logarithmic scale.

In the original manuscript we have already discussed *how the electric field penetration affects from high to low latitudes*. Namely, penetration of electric field is still a serious problem, and modern models can not provide strong electric field at $L < 1.3$ in order to explain observation of deep injections (e.g., Su et al., 2016; Selesnick et al., 2016). In Introduction and Discussion [lines 122-128; 647-652] we emphasized that:

“and most of researchers consider and model an electric drift of electrons in the ExB fields, even though the electric field must be very high (e.g., Zhao and Li, 2013; Turner et al., 2015; Lejosne and Mozer, 2016; Selesnick et al., 2016; Su et al., 2016; Zhao et al., 2017a). There is no explanation for penetration of a strong electric field to such low L -shells. empirical electric field models are limited and do not provide the results below $L \sim 2$ (e.g., Rowland and Wygant, 1998; Matsui et al., 2013). The most modern research suggests that the actual strength of penetration electric fields can be stronger than any existing electric field model at $L < 2$ (Su et al., 2016).”

“Another serious problem is the generation/penetration of electric fields in the inner magnetosphere, which is far from complete understanding. Numerical estimations show that the anomalous (fast) radial transport of particles observed in the inner magnetosphere can be produced by the electric field up to 5 mV/m (Selesnick et al., 2016; Suvorova et al., 2013). At the present time, there are no models predicting strong electric fields in the inner radiation belt and below.”

Specific Comment 5

5. Sorbo et al. (GRL, 2006) indicated the >30 keV electron flux enhancement in the NOAA/POES data at the equator caused by precipitation of energetic neutral atoms (ENAs). Although their events are mainly during magnetic storms, we can expect some amount of ENA flux even during quiet times, because ring current is a persistent feature in the magnetosphere. Is there any possibility that the present $L < 1.2$ electron flux enhancement is related to the ENAs from the magnetosphere?

Sørbo, M., F. Søråas, K. Aarsnes, K. Oksavik, and D. S. Evans (2006), Latitude distribution of vertically precipitating energetic neutral atoms observed at low altitudes, Geophys. Res. Lett., 33, L06108, doi:10.1029/2005GL025240.

Reply:

The ENA mechanism cannot explain very strong (3 order of magnitude) enhancements of the count rate in the channel of >30 keV electrons, which was observed during magnetic quiet (!) in a wide range of latitudes (~ 40 deg) and in a restricted range in longitudes. In particular, it is impossible to explain why almost whole Eastern hemisphere (longitudes from 0 to 160E) is free

from ENA. We even do not see there a small-amplitude equatorial maximum of ENA from the quiet ring current. Hence, this is certainly not the ring current effect.

Technical Corrections

6. line 120-122: *Please provide the values of the electric field suggested by these references.*

Reply:

We add the following :

“According to simulation results of Selesnick et al. (2016), the electric field of ~5 mV/m can provide deep injections at $L < 1.3$.”

7. line 182 (*kept at the enhanced level for several hours*): *Readers cannot understand how the authors obtain the information “several hours” from Figure 1b. Please explain.*

Reply:

We add this information in the next paragraph:

“Figure 2 and Table 1 present main characteristics of 15 FEE enhancements detected along equatorial passes of POES satellites (P2, P5, P6, P7, P8). The fluxes kept at the enhanced level for several hours. We analyze the peak fluxes in the FEE enhancements (time, local time, longitude, and L-shell).”

8. line 349-350 and line 462: *I think we cannot exclude the possibility of solar wind dynamic pressure variations, since the OMNI solar wind dynamic pressure in Figure 3a shows small variations with time scales well less than 1 hour throughout the plotted interval.*

Reply:

The OMNI data are obtained from measurements by the ACE and Wind upstream monitors. The ACE data were shown in Figure 8. The both datasets showed tenuous solar wind pressure variations of a few tenths of nPa around an average value 1.2 - 1.8. Figure 8 (b1, b2, b3) allow estimating the pressure variations more accurately (< 0.2 nPa). They cannot produce magnetic pulses with amplitude of ~10 nT. We check the both data further and find fast ~10% fluctuations of pressure with a quasi-period varying from ~2 to 10 min. The timescale of the magnetic pulses is much longer, from 15 min to ~1-1.5 h (Table 2). Hence, it is hard to connect fast pressure variations with the occasional magnetic pulses and shallow valleys presented in Figure 6. Moreover, small-scale fluctuations of the solar wind pressure could not produce intense precipitations observed in the cusp region (see Figure 11).

In the revised manuscript we add:

“Indeed, as one can see in Figures 1 and 8, tenuous variations of P_d do not exceed a few tenths of nPa and, thus, they cannot produce sharp geomagnetic pulses with amplitudes of ~10 nT.”

9. lines 528-529: *Why the authors focus only on night injections occurring occasionally from ~1300 to ~1700UT at 2-5 LT in Figure 2? There is a continuous injection at nearby 06 LT.*

Reply:

We replace “night” to “nightside” to avoid misunderstanding. Actually the “*continuous injection at nearby 06 LT*” occurred at around 5 LT (see Table 1). We analyzed 8 peak fluxes on the nightside at 1.8, 1.6, 5.1, 5.0 and 4.9 LT. They were listed as F1-F6 and F8, F10 in Table 1.

We revised the text accordingly:

“With analysis of longitudinal and local time distributions of the enhancements we identified a series of **nightside** injections occurred in the sector of 2 - 5 LT during the period from ~1300 to ~1700 UT (Figure 2).”

10. *Figure 3: I cannot see shaded box at 13-23 UT, which is mentioned in the figure caption.*

Reply:

We correct the Figure 3.

Sincerely,
Alla Suvorova